Time-Reversal based Detection in random media

Guillaume Bal * Olivier Pinaud †

May 17, 2005

Abstract

We consider the detection and imaging of inclusions buried in highly heterogeneous media. We assume that only the statistical properties of the heterogeneous media can be observed and that the wave energy density may be modeled by macroscopic equations. The detection and imaging capabilities hinge on ensuring that the measured data are statistically stable, which means that they depend only on the macroscopic statistical parameters of the random media and not on the microscopic statistical realization. In this paper, the macroscopic model is a diffusion equation. In this context, we construct statistical tests to detect inclusions based on macroscopic diffusion measurements and perform asymptotic expansions to image their location and volume. We show that time reversal measurements enjoy a much larger signal-to-noise ratio in the presence of background noise than do direct wave energy measurements. This is a direct consequence of the enhanced refocusing properties that characterize time reversed waves propagating in heterogeneous media. Finally we present numerical simulations of acoustic waves propagating in heterogeneous two-dimensional media. The numerical simulations illustrate which factors contribute to "noise" in the measured data and how they affect the detection and imaging capabilities.

1 Introduction

Waves emitted by a localized source, propagating in heterogeneous media for a certain time, recorded by an array of transducers, *time reversed*, and finally reemitted into the same media, enjoy striking refocusing properties in the vicinity of the original source namely, the tightness of the refocusing is very much enhanced when propagation occurs in highly heterogeneous media rather than in homogeneous media. This enhanced refocusing has been observed in many physical settings [24, 26, 29, 33]. It has also been analyzed mathematically in various regimes of wave propagation such as layered media [20, 31], directional regimes such as the paraxial or white noise regimes [6, 9, 16, 39], or more general multi-dimensional regimes based on radiative transport or Fokker-Planck

*Department of Applied Physics and Applied Mathematics, Columbia University, New York NY, 10027; gb2030@columbia.edu;

†Department of Applied Physics and Applied Mathematics, Columbia University, New York NY, 10027; op2102@columbia.edu

equations [8, 10, 11]. In all these regimes, the mechanism leading to *super-resolution*, in the sense that the signal focuses more tightly in heterogeneous media than in homogeneous media, is *multi-pathing*. The multi-pathing environment created by the heterogeneities may be characterized by macroscopic quantities that depend on the regime of wave propagation. In the regime of wave propagation of interest in this paper namely, that of radiative transfer and of its diffusion approximation, the super resolution is characterized by *filters*, who satisfy macroscopic equations, and whose smoothness properties indicate how tight the refocusing is [11]. A similar notion in directional regimes is that of *effective aperture* [16].

If one knows that a recorded signal propagating in heterogeneous media comes from a localized source, it is sufficient to time reverse it and send it back into the physical media: it will refocus at the source location. This has important applications in communication theory; see for instance [24, 26, 27]. It can also be used in detection and imaging of inclusions in cluttered media if the clutter is known *exactly*, i.e., if the Green function associated to the heterogeneous media is known [37]. In many practical settings however, the Green function is not known and the refocusing of time reversed waves cannot be used in a straightforward manner.

As it turns out, imaging modalities can benefit from another striking property of time reversed waves: *statistical stability*, which means that the macroscopic quantities characterizing multi-pathing are often functions of the *macroscopic* statistical properties of the random media and not of its *microscopic* statistical realization. The main effect is that the effective aperture in the paraxial regime or the filters in the transport regime characterizing time reversal are to a large extent statistically stable. This feature was successfully exploited in [17, 18] to modify imaging functionals so that they would be as independent as possible of the statistical fluctuations of the random media; see [25, 32] for other works on the use of time reversal in imaging in cluttered media.

The methods developed in [17, 18] exhibit far superior imaging capabilities than other classical techniques such as matched field. However, they still very much depend on the measurement of coherent signals. Such signals can indeed be measured in moderately noisy environments but fade away as randomness increases. It is precisely this configuration of very dense cluttering that we analyze in this paper. As was said earlier, imaging is still possible, even with very dense cluttering, when the full Green function is known. However, the accuracy to which we need to know the Green function is quite high. In a series of recent papers [1, 12, 13], it was shown that even quite small errors in the estimate of the Green function could very much perturb the refocusing properties of the time reversed signal. Sufficiently accurate knowledge of the media at the microscopic level is therefore out of reach in many interesting applications.

Let us assume that we want to do imaging in highly cluttered media whose properties are only known in a statistical sense. Since the wave field is highly oscillatory in such media, it is difficult to use it in the imaging process. Rather, a *macroscopic* description, modeling a macroscopic quantity that can be measured, is necessary. In this paper the macroscopic quantity is the wave energy density and the macroscopic model the diffusion equation. Most of the results presented in this paper may be generalized to other macroscopic models (such as for instance the radiative transfer equation [11] or the Fokker Planck equation [8]) although we shall only consider the diffusive model here for concreteness. Imaging and detection then depend on the inclusions' effect on

the constitutive parameter of the macroscopic model, which is the diffusion coefficient in the diffusive model. We thus replace an inverse problem based on the microscopic wave equation by an inverse problem based on the macroscopic diffusion equation. The physically accurate microscopic wave model is too sensitive to the heterogeneities of the underlying media, and is thus replaced it by a macroscopic model, whose role is to average out the unimportant fluctuations of the media and retain only its effective macroscopic features.

Imaging is thus based on fulfilling three main conditions. Firstly, we need to make sure that the macroscopic model is indeed an accurate description of the physical process. Secondly, we need to estimate the macroscopic statistical properties of the random media (the diffusion coefficient) in the presence and the absence of inclusions. Note that this is a much easier task than reconstructing the full Green function in heterogeneous media. Thirdly, we need to ensure that the macroscopic model is statistically stable. Indeed, the inverse problem associated to imaging in diffusive regimes requires us to obtain properties of a diffusion coefficient from energy measurements, a highly unstable (severely ill-posed) problem [5, 28]. It is therefore imperative to ensure that the measured macroscopic quantities are indeed functions of the macroscopic characteristics of the random media and not of its fluctuating microscopic realization.

This leaves us with the question of why time reversal may be useful. Whereas the filters characterizing time reversal indeed solve a diffusion equation [11], the energy density of classical waves propagating in diffusive media solves the same diffusion equation [40, 41] and can thus be used to probe fluctuations in the diffusion coefficient. The answer to why time reversed waves are superior to direct energy density measurements relies on quantifying the *background* noise. We will demonstrate that *direct* wave energy measurements and time reversal measurements have exactly the same imaging capabilities in the absence of background noise. What distinguishes them is *signal to (background) noise* (SNR) ratios. Waves propagating in diffusive environments decay very rapidly because of geometric spreading. The intensity measured at the array of detectors may therefore be relatively faint and of the same intensity as uncontrolled background noise. The relatively low SNR is then a serious impediment to the detection and imaging of inclusions. Time reversed waves, thanks to their highly efficient refocusing properties, are not so much affected by the background noise. The reason is the following. After a noisy signal is recorded and time reversed, the true signal will indeed refocus, that is, enjoy a sizeable spatial recompression, whereas the noise, which is incoherent with respect to the initial source term, will not. Time reversal has therefore this unique advantage that it significantly increases the signal-to noise ratio between the measured signal and the background noise. The situation is very similar in communication theory. Whereas multipathing is quite useful, and somewhat necessary, in multiple antenna communication devices, it also causes a lot of *fading* [30, 38], resulting in fairly low signal-to-noise ratios. In the regime of diffusion, using time reversal will have the same advantage as in imaging: it will enhance the signal-to-noise ratio and allow us to counteract the effects of fading. This enhanced signal-to-noise ratio may justify in practice the use of time reversal equipment, which allows us to measure the coherent structure of wave fields before time reversion and is therefore much more costly than what is needed in direct energy measurements.

The rest of the paper is structured as follows. Section 2 recalls the derivation ob-

tained in [11] to characterize the *filters*, which model the macroscopic features of time reversed waves in diffusive media. The detection and imaging procedure is then based on analyzing the fluctuations in the diffusion coefficient caused by buried inclusions. Section 3 recalls how the energy density of waves is modeled in the diffusive regime and characterizes the *direct* measurements that can be used towards imaging. In section 4, we present our main assumptions on the macroscopic diffusion model namely, that it is composed of a known background with constant diffusion coefficient and inclusions of small volume characterized by different diffusion coefficients. Because data are expected to be relatively noisy in practice, and because the reconstruction of diffusion coefficients from measurements is a highly unstable problem, low-dimensional parameterizations of the inclusions are necessary. The theory of small volume inclusions [3, 5, 19] is perfectly adapted to such situations. We generalize the asymptotic formulae developed in [19] to the time-dependent setting and characterize how the diffusive measurements (both direct and time reversal) are asymptotically affected by the presence of inclusions. Based on this asymptotic model for the available macroscopic measurements, we present in section 5 statistical tests whose objective is to minimize the error of missed detections based on a given level of false alarms. Section 6 is devoted to a careful analysis of the various noise levels that may affect the macroscopic measurements. We show that statistical stability is imperative for both the direct and the time reversal measurements, and that time reversal measurements are far less affected by background noises than direct measurements. We propose in section 7 numerical reconstructions in diffusive regimes based on various synthetic noise levels. We present in sections 8 and 9 numerical simulations of wave propagation in highly heterogeneous media and address in this setting the main aspects of the imaging techniques in diffusive regime introduced in earlier sections. In section 8, we present the two-dimensional numerical setting and show how the main constitutive parameters of diffusion equations can be estimated numerically. In section 9, we address the fundamental question of the statistical stability of measurements. We show that the statistical stability is not always guaranteed and indicate the type of measurements that should be performed to maximize stability. We also address detection and imaging capabilities at the end of the section. Concluding remarks are presented in section 10.

2 Time Reversal and Inverse Problem

Our model for wave propagation in random media will be that of acoustic waves. The generalization to other classical waves such as electromagnetic waves may be worked out as in [11]. The first order hyperbolic system for pressure $p(t, \mathbf{x})$ and velocity $\mathbf{v}(t, \mathbf{x})$ reads in this context:

$$\begin{aligned} &\frac{\partial \mathbf{v}}{\partial t} + \rho^{-1}(\mathbf{x}) \nabla p = 0, \\ &\frac{\partial p}{\partial t} + \kappa^{-1}(\mathbf{x}) \nabla \cdot \mathbf{v} = 0, \end{aligned} \tag{1}$$

with suitable initial conditions, where $\rho(\mathbf{x})$ is density and $\kappa(\mathbf{x})$ is compressibility of the underlying media. We recast the above system as

$$\frac{\partial \mathbf{u}}{\partial t} + A^{-1}(\mathbf{x}) D^j \frac{\partial \mathbf{u}}{\partial x^j} = 0, \tag{2}$$

where $\mathbf{u} = (\mathbf{v}, p)$ is a $4-$vector, $A = \mathrm{Diag}(\rho, \rho, \rho, \kappa)$ is a positive definite 4×4 diagonal matrix, and $D^j_{mn} = \delta_{m4}\delta_{nj} + \delta_{n4}\delta_{mj}$ is a 4×4 symmetric matrix for $1 \leq j \leq 3$. We use the Einstein convention of summation over repeated indices.

Time reversal consists then of two steps. We first let an acoustic signal propagate in the media for a duration $T > 0$:

$$\begin{aligned} &\frac{\partial \mathbf{u}}{\partial t} + A^{-1}(\mathbf{x}) D^j \frac{\partial \mathbf{u}}{\partial x^j} = 0, \qquad 0 < t < T, \\ &\mathbf{u}(0, \mathbf{x}) = \mathbf{S}(\mathbf{x}), \end{aligned} \tag{3}$$

where $\mathbf{S}(\mathbf{x})$ is a localized source centered at $\mathbf{x}_0$, which to simplify we assume is irrotational, i.e., of the form $\mathbf{S}(\mathbf{x}) = (\nabla \phi_0(\mathbf{x}), p_0(\mathbf{x}))^t$ for some potential ϕ_0 and pressure p_0. Such an initial condition may be obtained physically by sending a superposition of temporal pulses. For instance, we may consider the equation

$$\frac{\partial \mathbf{u}}{\partial t} + A^{-1}(\mathbf{x}) D^j \frac{\partial \mathbf{u}}{\partial x^j} = \mathbf{S}(\mathbf{x}) \frac{1}{\varepsilon} \psi(\frac{t+\varepsilon}{\varepsilon}), \quad t \in \mathbb{R}, \quad \mathbf{x} \in \mathbb{R}^3, \tag{4}$$

where $\psi(t)$ is a non-negative smooth function supported on $(0, 1)$ such that $\int_0^1 \psi(t) dt = 1$. We may then verify that for the type of underlying media of interest to us, the solution to (4) verifies

$$\mathbf{u}(0, \mathbf{x}) = \mathbf{S}(\mathbf{x}) + \text{lower-order term in } \varepsilon. \tag{5}$$

The signal is then recorded by an array of receivers modeled by a function $\chi_\Omega(\mathbf{x})$ (such that $\chi_\Omega(\mathbf{x}) = 0$ when there is no detector at $\mathbf{x}$). The recording occurs over a time window modeled by $\chi_\tau(t)$. After the full signal has been recorded, it is digitally time reversed, which here corresponds to multiplying it by the matrix $\Gamma = \mathrm{Diag}(-1, -1, -1, 1)$. This means that pressure is kept unchanged and that the sign of the velocity field is reversed. The time reversed recorded signal is thus given by

$$\tilde{\mathbf{R}}(t, \mathbf{x}) = \chi_\tau(t) \mathbf{R}(t, \mathbf{x}), \qquad \text{where} \quad \mathbf{R}(t, \mathbf{x}) = \Gamma \mathbf{u}(t, \mathbf{x}) \chi_\Omega(\mathbf{x}). \tag{6}$$

In a second step, the time reversed recorded signal is emitted back into the *same* media, knowing that what was recorded last is sent back first. This yields the following modeling:

$$\begin{aligned} &\frac{\partial \mathbf{u}}{\partial t} + A^{-1}(\mathbf{x}) D^j \frac{\partial \mathbf{u}}{\partial x^j} = \chi_\tau(2T - t) \mathbf{R}(2T - t, \mathbf{x}), \quad T \leq t \leq 2T, \\ &\mathbf{u}(T, \mathbf{x}) = 0. \end{aligned} \tag{7}$$

By superposition, the back-propagated signal is then given by

$$\mathbf{u}(2T, \mathbf{x}) = \int_0^T \mathbf{w}(s, \mathbf{x}; s) \chi_\tau(s) ds, \tag{8}$$

where the function $\mathbf{w}(s, \mathbf{x}; s)$ solves the problem

$$\begin{aligned} &\frac{\partial \mathbf{w}}{\partial t} + A^{-1}(\mathbf{x}) D^j \frac{\partial \mathbf{w}}{\partial x^j} = 0, \quad 0 \leq t \leq s, \\ &\mathbf{w}(0, \mathbf{x}; s) = \mathbf{R}(s, \mathbf{x}). \end{aligned} \tag{9}$$

Understanding the refocusing properties of the *single-time* time reversed signal $\mathbf{w}(s,\mathbf{x};s)$ is therefore sufficient to analyze the back-propagated signal $\mathbf{u}(2T,\mathbf{x})$ by superposition.

We are interested in signals propagating over distances L much larger than the typical wavelength of the initial condition: $\varepsilon = \lambda/L \ll 1$. The time T is also of order L/c_0, where c_0 is the average speed of propagation in the media. In adimensionalized quantities $\mathbf{x}/L$ and t/T, we thus consider initial conditions of the form

$$\mathbf{u}(0,\mathbf{x}) = \varepsilon^{-3/2}\mathbf{S}\Big(\frac{\mathbf{x}-\mathbf{x}_0}{\varepsilon}\Big) \equiv \mathbf{S}_\varepsilon\Big(\frac{\mathbf{x}-\mathbf{x}_0}{\varepsilon}\Big), \tag{10}$$

where $\mathbf{x}_0$ is the average location of the source and where the factor $\varepsilon^{-3/2}$ has been added so that the energy of $\mathbf{u}(0,\mathbf{x})$ is independent of ε. The back-propagated signal will also refocus in the vicinity of $\mathbf{x}_0$ and we consequently introduce the notation

$$\mathbf{u}^B(\boldsymbol{\xi};\mathbf{x}_0) = \Gamma\mathbf{u}(2T,\mathbf{x}_0+\varepsilon\boldsymbol{\xi}). \tag{11}$$

We have multiplied the back-propagated signal by the time reversal matrix Γ for the following reason: assuming that $\chi_\tau(t) = \delta(t-T_0)$ and that $\chi_\Omega(\mathbf{x}) \equiv 1$ so that the whole signal is recorded at time T_0; we can then verify that $\mathbf{u}^B(\boldsymbol{\xi};\mathbf{x}_0) = \varepsilon^{-3/2}\mathbf{S}(\boldsymbol{\xi})$. This property is ensured by the reversibility in time of the hyperbolic system (2).

One of the striking properties of time reversed signal is that their refocusing is greatly enhanced by the presence of a highly heterogeneous underlying media. Such a behavior has been explained for several models of heterogeneous media. A quite satisfactory model that accounts for the diversity of the wave energy density, both in space and in wavenumbers, is that of radiative transfer equations [11, 40] and its approximation by diffusion equations. We shall focus in this paper on the model of diffusion equations for its relative simplicity.

Let us assume that measurements are performed at a single time so that $\chi_\tau(t) = \delta(t-T_0)$. The theory developed in [11] then tells us that asymptotically, as $\varepsilon \to 0$, the back-propagated signal is related to the source term according to the relation

$$\mathbf{u}^B(\boldsymbol{\xi};\mathbf{x}_0) = \big(\mathbf{F}(T_0,\cdot;\mathbf{x}_0) * \mathbf{S}_\varepsilon(\cdot)\big)(\boldsymbol{\xi}), \tag{12}$$

which upon taking Fourier transforms in the $\boldsymbol{\xi}$ variable only (defined in the sequel as $\hat{f}(\mathbf{k}) = \int_{\mathbb{R}^3} e^{-i\mathbf{k}\cdot\boldsymbol{\xi}} f(\boldsymbol{\xi})d\boldsymbol{\xi}$), yields the equivalent relation

$$\hat{\mathbf{u}}^B(\mathbf{k};\mathbf{x}_0) = \hat{\mathbf{F}}(T_0,\mathbf{k};\mathbf{x}_0)\hat{\mathbf{S}}_\varepsilon(\mathbf{k}). \tag{13}$$

The *Filter* $\hat{\mathbf{F}}(T_0,\mathbf{k};\mathbf{x}_0) = F(T_0,\mathbf{x}_0,|\mathbf{k}|)I$ is a 4×4 matrix proportional to Identity, where the coefficient of proportionality $F(T_0,\mathbf{x}_0,|\mathbf{k}|)$ solves the following diffusion equation

$$\begin{aligned} &\frac{\partial F}{\partial t} - D(|\mathbf{k}|)\Delta_{\mathbf{x}}F = 0, \\ &F(0,\mathbf{x},|\mathbf{k}|) = \chi_\Omega(\mathbf{x}). \end{aligned} \tag{14}$$

We refer to [11, 40] for details on the derivation of the equation for F and the definition of the diffusion coefficient $D(|\mathbf{k}|)$; see also (54) and (56) in section 8. The diffusion coefficient is inversely proportional to the power spectrum of the fluctuations of the heterogeneous media modeled by $\rho(\mathbf{x})$ and $\kappa(\mathbf{x})$.

When the underlying media is rigorously statistically homogeneous (i.e., its statistics do not depend on position), then the diffusion coefficient $D(|\mathbf{k}|)$ is indeed independent of any spatial variable and only depends on the wavenumber of the propagating waves. We now assume that the underlying media is statistically homogeneous, but only "locally" at the macroscopic scale, so that the resulting diffusion coefficient becomes a function of position as well: $D(\mathbf{x}, |\mathbf{k}|)$. The "local" statistical homogeneity only makes sense if the statistical properties of the underlying media change at the *macroscopic* scale $\mathbf{x}$ and are indeed homogeneous at the *microscopic* scale $\varepsilon\mathbf{x}$. In that case, the theory developed in [11, 40] may be formally generalized to obtain that the filter F solves the following equation

$$\begin{aligned} &\frac{\partial F}{\partial t} - \nabla \cdot D(\mathbf{x}, |\mathbf{k}|)\nabla F = 0, \\ &F(0, \mathbf{x}, |\mathbf{k}|) = \chi_\Omega(\mathbf{x}). \end{aligned} \tag{15}$$

Our objective in this paper is to use the enhanced refocusing properties of time reversed waves to detect spatial variations in the diffusion coefficient $D(\mathbf{x}, |\mathbf{k}|)$.

Collecting the results obtained above, finally we can characterize the backpropagated signal $\mathbf{u}^B(\boldsymbol{\xi}; \mathbf{x}_0)$ as

$$\hat{\mathbf{u}}^B(\mathbf{k}; \mathbf{x}_0) = \int_0^T F(t, \mathbf{x}_0, |\mathbf{k}|)\hat{\mathbf{S}}_\varepsilon(\mathbf{k})\chi_\tau(t)dt, \tag{16}$$

where $F(t, \mathbf{x}_0, |\mathbf{k}|)$ is the solution of (15). To simplify the analysis, we shall assume that $\chi_\tau(t) = \delta(t - T^-)$ so that $\hat{\mathbf{u}}^B(\mathbf{k}; \mathbf{x}_0) = F(T, \mathbf{x}_0, |\mathbf{k}|)\hat{\mathbf{S}}_\varepsilon(\mathbf{k})$. Our *data*, on which the detection will be based, are thus local values or moments (integrated quantities) of

$$F(T, \mathbf{x}_0, |\mathbf{k}|) = \frac{\hat{\mathbf{u}}^B(\mathbf{k}; \mathbf{x}_0)}{\hat{\mathbf{S}}_\varepsilon(\mathbf{k})}. \tag{17}$$

By measuring the above quantity for various wavenumbers $|\mathbf{k}|$, positions $\mathbf{x}_0$, and experiment durations T, we collect information about the solution of (15) from which we want to obtain information about the diffusion coefficient $D(\mathbf{x}, |\mathbf{k}|)$.

3 Direct measurements and Inverse Problem

In the previous section, we saw how the backpropagated signal was related to the original source term $\mathbf{S}(\mathbf{x})$ via (16). The derivation was based on the diffusion theory, which can also be used to model the energy density of waves propagating in heterogeneous media.

Indeed let us consider the (acoustic) energy

$$\mathcal{E}(t, \mathbf{x}) = \frac{1}{2}\mathbf{u}(t, \mathbf{x}) \cdot A(\mathbf{x})\mathbf{u}(t, \mathbf{x}) = \frac{1}{2}\Big(\rho(\mathbf{x})|\mathbf{v}(t, \mathbf{x})|^2 + \kappa(\mathbf{x})p^2(t, \mathbf{x})\Big). \tag{18}$$

In the diffusive regime, both terms in the above equation are actually equal (equipartition between the kinetic energy and the potential energy) and the energy density takes the form

$$\mathcal{E}(t, \mathbf{x}) = \int_0^\infty U(t, \mathbf{x}, |\mathbf{k}|)4\pi|\mathbf{k}|^2 d|\mathbf{k}|, \tag{19}$$

where $U(t, \mathbf{x}, |\mathbf{k}|)$ solves the following equation

$$\begin{aligned} &\frac{\partial U}{\partial t} - \nabla \cdot D(\mathbf{x}, |\mathbf{k}|)\nabla U = 0, \\ &U(0, \mathbf{x}, |\mathbf{k}|) = \frac{\delta(\mathbf{x} - \mathbf{x}_0)}{2(2\pi)^6} \int_{S^2} \hat{\mathbf{S}}(|\mathbf{k}|\hat{\mathbf{k}}) \cdot A(\mathbf{x}_0)\hat{\mathbf{S}}(|\mathbf{k}|\hat{\mathbf{k}}) \frac{d\hat{\mathbf{k}}}{4\pi}. \end{aligned} \tag{20}$$

Here we have used the notation $\mathbf{k} = |\mathbf{k}|\hat{\mathbf{k}}$. The energy density $\mathcal{E}(t, \mathbf{x})$ does not quite solve a closed form equation. However, it may be decomposed according to (19), where each component satisfies a diffusion equation of the form (20).

Since (19) and (20) do not appear explicitly in the literature, we briefly derive them from the material in [40]. The derivation of (19) and (20) follows from the projection of the Wigner transform of the initial condition $\mathbf{S}_\varepsilon(\mathbf{x})$ onto the propagating mode as is done in (3.41), (3.42), and (3.47) of [40]. Because of the specific form of the initial condition $\mathbf{S}^\varepsilon = (\varepsilon\nabla\phi_0^\varepsilon, p_0^\varepsilon)^t = \varepsilon^{-3/2}(\varepsilon\nabla\phi_0(\frac{\mathbf{x}-\mathbf{x}_0}{\varepsilon}), p_0(\frac{\mathbf{x}-\mathbf{x}_0}{\varepsilon}))$, the projection of the Wigner transform of $\mathbf{S}_\varepsilon(\mathbf{x})$ onto the propagating mode reads

$$a_\varepsilon^+(0, \mathbf{x}, \mathbf{k}) = \int_{\mathbb{R}^3} e^{i\mathbf{k}\cdot\mathbf{y}} f^\varepsilon\left(\mathbf{x}, \mathbf{x} - \frac{\varepsilon\mathbf{y}}{2}, \mathbf{k}\right) f^\varepsilon\left(\mathbf{x}, \mathbf{x} + \frac{\varepsilon\mathbf{y}}{2}, \mathbf{k}\right) \frac{d\mathbf{y}}{(2\pi)^3},$$

where $f^\varepsilon(\mathbf{x}, \mathbf{z}, \mathbf{k}) = \sqrt{\frac{\rho(\mathbf{x})}{2}}(\varepsilon\nabla\phi_0^\varepsilon(\mathbf{z}) \cdot \hat{\mathbf{k}}) + \sqrt{\frac{\kappa(\mathbf{x})}{2}} p_0^\varepsilon(\mathbf{z})$. As $\varepsilon \to 0$, we find the limit

$$a^+(0, \mathbf{x}, \mathbf{k}) = \frac{\delta(\mathbf{x} - \mathbf{x}_0)}{(2\pi)^6}\left(\frac{\rho}{2}|i\mathbf{k}\hat{\phi}_0(\mathbf{k})|^2 + \frac{\sqrt{\kappa\rho}}{2} i|\mathbf{k}|(\hat{\phi}_0(\mathbf{k})\hat{p}_0(-\mathbf{k}) - \hat{\phi}_0(-\mathbf{k})\hat{p}_0(\mathbf{k})) + \frac{\kappa}{2}|\hat{p}_0(\mathbf{k})|^2\right).$$

The initial conditions for the diffusion equation are then given by the average over $\hat{\mathbf{k}}$ of the above $a^+(0, \mathbf{x}, \mathbf{k})$. This is the initial condition given in (20).

The energy density corresponding to the initial conditions $\hat{\mathbf{S}}_\varepsilon(\mathbf{k})$ concentrated at one frequency $\omega = c_0|\mathbf{k}|$ therefore solves the same equation as the filters obtained in (17). We can thus directly use the measurements $\chi_\Omega(\mathbf{x})U(T, \mathbf{x}, |\mathbf{k}|)$ to probe the media and detect the presence of inclusions. In the idealized -though practically quite relevant- case where both the source term and the array of detectors are localized at the macroscopic location $\mathbf{x}_0$ (although both are large compared to the microscopic scale $\varepsilon\mathbf{x}$), then both the time reversal and direct measurements provide the *same* information about the media: the solution $U(T, \mathbf{x}_0, |\mathbf{k}|)$ at various times T. One may consequently wonder what advantage there is to using the data obtained in (17) by the time reversal experiment rather than the *direct* measurements. In the absence of external noise in the data, the answer we have just obtained is simple: none whatsoever. In the presence of external noise however, the reconstruction very much depends on the signal to noise ratio, modeled by $U(t, \mathbf{x}, |\mathbf{k}|)/\mathcal{N}_D$ for direct measurements and by $F(t, \mathbf{x}, |\mathbf{k}|)/\mathcal{N}_{TR}$ for time reversal measurements. We shall see in section 6 that the signal to noise ratio may indeed be much higher for time reversal measurements than it is for direct measurements, whereby justifying the use of time reversal based procedures to enhance detection and imaging.

4 Characteristics of media and inclusions

The theory presented in the preceding sections to model the available *measurements* fundamentally modifies the detection problem. We started with a microscopic wave

model, where the background and the inclusions were modeled by variations in the density and the compressibility parameters and arrived at a macroscopic diffusion model for the wave energy density, where the background and the inclusions are modeled by a spatially varying diffusion coefficient.

We may justify this as follows. Because of the highly heterogeneous character of the underlying media, there is little hope that wave measurements may be successfully used to detect the inclusions. Indeed, in the regime leading to the diffusion approximation, coherent signals are exponentially damped by the heterogeneities. Algorithms based on the coherent information, such as travel time estimates or matched field, cannot be efficient in such regimes.

Detection must therefore rely on the incoherent structure of the waves. This incoherent structure is not arbitrary. In many regimes, we can make sense of macroscopic quantities, such as the energy density of waves and obtain macroscopic closed form equations for them. The diffusive regime provides an example of such a macroscopic equation. When such a regime can be exhibited, it is clearly advantageous to use it for the detection problem as well. This is the point of view we have taken in this paper. Rather than modeling inclusions at the microscopic level as fluctuations in the sound speed, we model them at the macroscopic level as spatial fluctuations in the diffusion coefficient.

There is a vast literature on the inversion of diffusion coefficients in parabolic equations and in elliptic equations, its steady-state counterpart; see [3, 28, 34, 36]. One of their main characteristics is their severe ill-posedness, which imply that small errors in the data may have very large repercussions on the quality of the reconstruction of $D(\mathbf{x})$. In this paper, we restrict ourselves to the detection problem of localized inclusions. We assume that the background is known, so that in the absence of inclusions, $D(\mathbf{x}) = D_0$, a constant to simplify. This implies that the *statistical* properties of the underlying media are known in the absence of inclusion. This, however, clearly does not mean that the underlying media is completely known, which would imply knowledge of the Green function associated to (2). As we have already mentioned, detection is much simplified when full knowledge of the Green function is available [37].

Our second assumption concerns the inclusions. We are typically interested in detection based on only a few measurements of $F(T, \mathbf{x}_0, |\mathbf{k}|)$, for instance at fixed $|\mathbf{k}|$, for a given judiciously chosen T, and at a few source locations $\mathbf{x}_0$. Since the reconstruction of the diffusion coefficient is an ill-posed inverse problem, drastic assumptions on the diffusion coefficient are necessary. An interesting framework, not very different from the point-scatterer approximation used in detection based on coherent signals, is that of localized inclusions with arbitrary contrast in their diffusive properties but small volume. Truncated asymptotic expansions in the volume provide us with a finite number of parameters that one can reconstruct from moderately noisy measured data. In many situations, they also provide us with the correct information on which detection tests should be based.

In both cases of time reversal (see (15)) and direct (see (20)) measurements, the measured data are modeled by a diffusion equation of the form

$$\begin{aligned} &\frac{\partial u}{\partial t}(t, \mathbf{x}) - \nabla \cdot D(\mathbf{x}) \nabla u(t, \mathbf{x}) = 0, \qquad t > 0, \\ &u(0, \mathbf{x}) = u_{\text{in}}(\mathbf{x}). \end{aligned} \tag{21}$$

We assume that $\mathbf{x} \in \mathbb{R}^d$ for $d = 2, 3$ and do not prescribe any boundary conditions to simplify. We consider the detection and imaging of a single inclusion, although the generalization to multiple inclusions is theoretically straightforward, and assume that the inclusion is a ball of radius R. The inclusion is thus modeled by its location $\mathbf{x}_b$, its radius R, and its diffusion coefficient D_1. We recall that the background is modeled by a diffusion coefficient $D(\mathbf{x}) = D_0$, which we assume to be known.

Provided that the radius is sufficiently small compared to the main distance of propagation, $R \ll L$, where (after appropriate rescaling) $L \sim O(1)$ is the typical macroscopic scale of the domain of propagation, we can devise an asymptotic expansion for the solution of (21) in powers of the radius R. Note that the radius of the inclusion still needs to be very large compared to the transport mean free path $\Sigma^{-1}(k)$, where $\Sigma(k)$ is defined in (54) below, in order for the diffusion approximation to hold. Asymptotic expansions were first obtained in [19] for the steady-state problem and later extended to other frameworks; see [3] for a recent reference. In the context of the parabolic equation (21), the asymptotic expansion takes the following form. Let $u_0(t, \mathbf{x})$ be the solution of the unperturbed problem, where $D(\mathbf{x}) = D_0$ for all $\mathbf{x} \in \mathbb{R}^d$, and let $G(t, \mathbf{x}, \mathbf{x}_b)$ be the fundamental solution of the same equation with initial conditions $\delta(\mathbf{x} - \mathbf{x}_b)$ (the Green function depends on possible imposed boundary conditions). Let finally $\delta u(t, \mathbf{x}) = u(t, \mathbf{x}) - u_0(t, \mathbf{x})$. Then we have

$$\begin{aligned} \delta u(t, \mathbf{x}) &= D_0 R^d \int_0^t \nabla_{\mathbf{x}} u_0(t - s, \mathbf{x}_b) \cdot M \nabla_{\mathbf{x}_b} G(s, \mathbf{x}, \mathbf{x}_b) ds + O(R^{d+1}) \\ M &= d\pi \frac{D_0 - D_1}{(d-1)D_0 + D_1} \, I_d. \end{aligned} \tag{22}$$

The second-order tensor M is called the polarization tensor. The error estimate in $O(R^{d+1})$ is quite conservative; see [3]. Here is a brief derivation of the above formula based on what exists in the literature. The Laplace transform $\check{u}(\omega, \mathbf{x})$ of $u(t, \mathbf{x})$ in the time variable on $\mathbb{R}^+$ satisfies the equation

$$-\nabla \cdot D(\mathbf{x}) \nabla \check{u}(\omega, \mathbf{x}) + \omega \check{u}(\omega, \mathbf{x}) = u_{\text{in}}(\mathbf{x}).$$

We may now use the classical formulae in [3, 19] to deduce that

$$\delta \check{u}(\omega, \mathbf{x}) = D_0 R^d \nabla_{\mathbf{x}} \check{u}_0(\omega, \mathbf{x}_b) \cdot M \nabla_{\mathbf{x}_b} \check{G}(\omega, \mathbf{x}, \mathbf{x}_b) + O(R^{d+1}),$$

where $\delta \check{u}$, $\check{u}_0$, and $\check{G}$ are the Laplace transforms of δu, u_0, and G in the time variable, respectively, and where the polarization tensor M is defined as in (22). It suffices to take the inverse Laplace transform in the above equation to obtain (22).

Because we are interested in relatively small inclusions in practice, the above formula may often prove sufficient. The expansion in powers of R can be pushed further to obtain additional information about the inclusion, as was done in [3, 5]. The latter reference shows however that more refined information on the inclusions than that retrievable from (22) requires quite accurate data, which may not be available in practice.

5 Statistical tests

The asymptotic formula (22) allows us to acquire knowledge about the presence or not of an inclusion. In this section we are interested in testing the hypothesis whether the

presence of an inclusion is compatible with the measured data. We first assume that we have access to one measurement $\delta u = \delta u(t, \mathbf{x}_m)$ for a given time t and location $\mathbf{x}_m$.

Let us assume that $\mathbf{x}_m = \mathbf{x}_0$, which corresponds to the echo mode. In the absence of noise, we can detect an inclusion less diffusive than the background media if we observe that $\delta u < 0$ and can detect an inclusion more diffusive than the background provided that $\delta u > 0$. We shall simplify the presentation by assuming that $D_1 = +\infty$. This corresponds to a perfectly homogeneous inclusion (the power spectrum of the heterogeneities vanishes within the inclusion). Because energy can propagate more freely within the inclusion than in the background, we expect to observe a drop of energy $\delta u(t, \mathbf{x}_m) < 0$ in the echo mode.

In practice, the measured data $\delta\tilde{u}(t, \mathbf{x}_m)$ differ from the model $\delta u(t, \mathbf{x}_m)$ because of the presence of uncertainties. In the present case, we can distinguish two types of uncertainties. The first one is classical and models measurement errors at the detectors. These errors may be caused by defects in the detectors or by a "background noise". The latter will be important to distinguish the detection capabilities of time reversal when compared to direct energy measurements. We will model this error at the detector array as an additive noise with Gaussian statistics $n_{\mathrm{d}} \sim \mathcal{N}(0, \sigma_{\mathrm{d}}^2)$.

The second type of error pertains to the accuracy of the diffusive model itself. The diffusion equations recalled in earlier sections are valid in the high-frequency limit only. At fixed ε, their validity holds only in an approximate sense, and the error may very much depend on the realization of the random media used to model wave propagation. It seems realistic to model this error as a multiplicative noise, and for want of a better statistical model, we shall also assume that the noise has Gaussian statistics: $n_{\mathrm{m}} \sim \mathcal{N}(0, \sigma_{\mathrm{m}}^2)$. This noise will be defined more carefully in a later section.

Upon compounding these errors, we may relate our measurements to the true model as

$$\delta\tilde{u} = \delta u(t, \mathbf{x}_m; R, \mathbf{x}_b) + n = R^d \delta u(t, \mathbf{x}_m; 1, \mathbf{x}_b) + n, \tag{23}$$

where $n \sim \mathcal{N}(0, \sigma^2)$ for some $\sigma > 0$. Here t and $\mathbf{x}_m$ are fixed. The parameters R and $\mathbf{x}_b$ are yet unknown. Constructing a test for such a model is classical. The test is based on two hypotheses

- H_0: hypothesis that there is no inclusion (null hypothesis).
- H_A: hypothesis that there is an inclusion (alternate hypothesis).

We want to test H_0 against H_A. Two types of independent errors can be made. Type I errors correspond to rejecting H_0 when it is correct (false alarm). Their probability is given by:

$$\alpha = P(\text{rejecting } H_0 | H_0 \text{ is true}), \tag{24}$$

also called the level of significance of the test. Type II errors correspond to accepting H_0 when it is false (missed detection) and have probability

$$\beta = P(\text{accepting } H_0 | H_A \text{ is true}). \tag{25}$$

The success of the test (probability of detection) is therefore given by

$$\text{Power of the test } = 1 - \beta. \tag{26}$$

Let us assume that the inclusion is non-scattering $D_1 = \infty$ so that $\delta u < 0$. The test is then based on the signal to noise ratio. When $-\delta u$ is much larger than σ, we want to conclude that there is an inclusion. This implies the existence of a threshold above which we reject the null hypothesis. Such a threshold may be obtained as follows.

We want to construct a test that minimizes the probability of Type II error (probability of missed detection) for a given level of confidence of Type I error (false alarms). Such optimal tests are called *most powerful* [23]. The answer to such a problem is given by the Neyman Pearson lemma. Let us assume that $(R, \mathbf{x}_b)$ are known so that H_A is a non-composite hypothesis. We thus wish to know whether the data $-\delta\tilde{u}$ was drawn from the null distribution $\mathcal{N}(0, \sigma^2)$ or from the alternate distribution $\mathcal{N}(\mu, \sigma^2)$ with $\mu = -\delta u(R, \mathbf{x}_b) \geq 0$. The corresponding likelihoods $l_0(x)$ and $l_A(x)$ are given by

$$l_0(x) = \frac{1}{\sqrt{2\pi}\sigma} e^{-\frac{x^2}{2\sigma^2}}, \qquad l_A(x) = \frac{1}{\sqrt{2\pi}\sigma} e^{-\frac{(x-\mu)^2}{2\sigma^2}}. \tag{27}$$

The likelihood ratio is then given by

$$\Lambda(x) = \frac{l_A(x)}{l_0(x)} = e^{-\frac{\mu^2}{2\sigma^2}} e^{\frac{\mu x}{\sigma^2}}. \tag{28}$$

We deduce from the Neyman-Pearson lemma that all the tests that minimize Type II errors for a given Type I error are automatically of the form

$$\begin{array}{lll} \text{Reject} & H_0 & \text{if} \quad \Lambda(-\delta\tilde{u}) > \eta, \\ \text{Accept} & H_0 & \text{otherwise}, \end{array} \tag{29}$$

for some threshold $\eta > 0$. The relationship between η and α is given by

$$\int_{\Lambda(x)>\eta} l_0(x)dx = \alpha. \tag{30}$$

The calculations may be simplified by remarking that the log of the likelihood ratio in (28) is affine in x so that tests of the form $\Lambda(x) > \eta$ are equivalent to tests of the form $x > \tau$ for a suitable $\tau > 0$. Let $\Phi(x)$ be the (cumulative) distribution function of the random variable $X = \mathcal{N}(0, 1)$, i.e., $\Phi(x) = P\{X \leq x\}$. The test (29) may thus be recast as

$$\begin{array}{lll} \text{Reject} & H_0 & \text{if} \quad -\delta\tilde{u} > \tau, \\ \text{Accept} & H_0 & \text{otherwise}, \end{array} \tag{31}$$

where

$$\alpha = \int_{x>\tau} l_0(x)dx = \int_{x>\tau/\sigma} l_0(\sigma x)d(\sigma x) = 1 - \Phi\Big(\frac{\tau}{\sigma}\Big). \tag{32}$$

The relation $\alpha = \alpha(\tau)$ may be inverted to give

$$\tau(\alpha; \sigma) = \sigma\Phi^{-1}(1 - \alpha). \tag{33}$$

The threshold $\tau(\alpha; \sigma)$ does not depend on the inclusion's properties $(R, \mathbf{x}_b)$. The test is therefore optimal (*uniformly most powerful* (UMP) in the statistical literature) independent of the inclusion.

The power of the test however, certainly depends on the inclusion's properties. By definition, it is given by

$$1-\beta=\int_{\Lambda(x)>\eta} l_A(x)dx=\int_{x>\tau} l_A(x)dx=1-\Phi\Big(\frac{\tau(\alpha;\sigma)+R^d\delta u(1;\mathbf{x}_b)}{\sigma}\Big). \tag{34}$$

We observe that $1-\beta$ is an increasing function in $-R^d\delta u(1;\mathbf{x}_b)$ converging to α as $-R^d\delta u(1;\mathbf{x}_b)\to 0$ (corresponding to small objects or objects very far $|\mathbf{x}_b|\gg 1$), and converging to 1 as $-R^d\delta u(1;\mathbf{x}_b)\to\infty$.

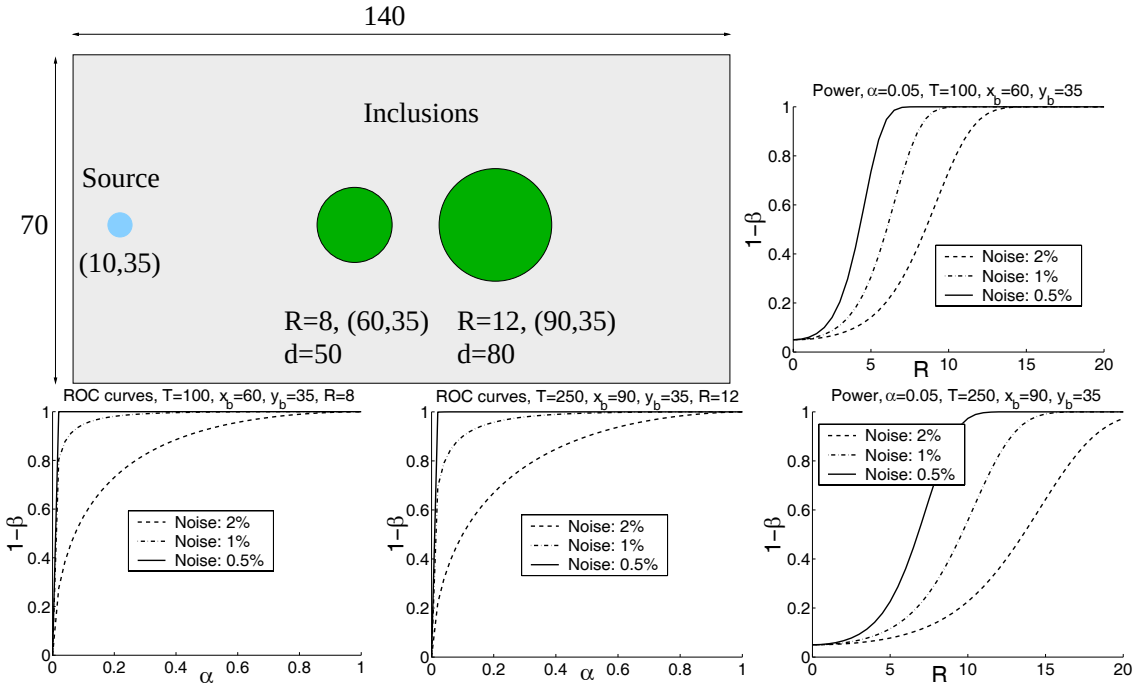

Figure 1: Power of the statistical test (31) for measurements $\delta\tilde{u}$ given in (23) based on (22) for the diffusion solution. The measurements are performed for two inclusions and three noise levels given in percentage of $u_0(T,\mathbf{x}_m)$. Top-left: geometry of the two inclusions. Measurements are performed at the source location (a peaked Gaussian in the simulations) $\mathbf{x}_m=\mathbf{x}_0=(10,35)$. Bottom two left pictures: ROC curves for the two inclusions (power of the test as a function of α) for different noise levels. Right row: power of the test as a function of the radius R of the inclusion for a fixed $\alpha=0.05$. In all simulations, the background diffusion is $D_0=23$ and the inclusion's diffusion $D_1=+\infty$. For the inclusion at $d=50$, we have chosen $T=100$ and for the inclusion at $d=80$, $T=250$.

The above formula (34) is quite classical. A common means of displaying the power is with the *receiver operating characteristic* (ROC) curve. We plot this probability of detection versus the probability of false alarm in Fig. 1 for various inclusions and noise levels. We also plot the probability of detection for a given $\alpha=0.05$ as a function of the radius R. We use arbitrary units in this section. One unit of distance corresponds to one wavelength and one unit of time to one wave period (with effective sound speed equal to 1) in section 9 devoted to the numerical simulation of wave equations. In such arbitrary

units, the background coefficient $D_0 = 23$ has been chosen to match those obtained in later sections. Note that the measurements performed at the source location and may correspond to direct measurements or time reversal measurements. For the inclusion at $d = 50$, time $T = 100$ maximizes the fluctuation $\delta u/u_0$ (on the order of 2%). For the inclusion $d = 80$, time $T = 250$ is roughly 25% larger than the time that maximizes the fluctuation $\delta u/u_0$ (on the order of 1.8%). In both cases, d measures the distance between the source and the inclusion's center.

Case of multiple measurements. Let us now consider the case of multiple measurements. We still assume that T is fixed and consider measurements at different locations $\mathbf{x}_m$ for $1 \leq m \leq M$. The inclusion will still be of the form $D_1 = +\infty$ and we assume that $\delta u(t, \mathbf{x}_m) < 0$ for all $\mathbf{x}_m$. In the case of infinite media, this is equivalent to having $(\mathbf{x}_m - \mathbf{x}_b) \cdot (\mathbf{x}_0 - \mathbf{x}_b) > 0$, $\mathbf{x}_0$ is the source location, for all $1 \leq m \leq M$.

We assume that the noise contributions at different locations $\mathbf{x}_m$ are uncorrelated. We can thus model the measurements as

$$-\delta\tilde{u}_m \sim \mathcal{N}(R^d \mu_m, \sigma_m^2), \qquad \mu_m = -\delta u_m(t, \mathbf{x}_m; 1, \mathbf{x}_b). \tag{35}$$

Let us define

$$\boldsymbol{x} = (-\delta\tilde{u}_m)_{1\leq m\leq M}, \quad \boldsymbol{\mu} = (\mu_m)_{1\leq m\leq M}, \quad \Sigma = \mathrm{Diag}(\sigma_1^2, \ldots, \sigma_M^2). \tag{36}$$

We wish to test H_0 against the alternative H_A. The corresponding likelihoods take the form

$$l_0(\boldsymbol{x}) = \frac{\exp\big(-\frac{1}{2}\boldsymbol{x}\cdot\Sigma^{-1}\boldsymbol{x}\big)}{\sqrt{2\pi}|\mathrm{det}\Sigma|^{1/2}}, \qquad l_A(\boldsymbol{x}) = \frac{\exp\big(-\frac{1}{2}(\boldsymbol{x}-R^d\boldsymbol{\mu})\cdot\Sigma^{-1}(\boldsymbol{x}-R^d\boldsymbol{\mu})\big)}{\sqrt{2\pi}|\mathrm{det}\Sigma|^{1/2}}, \tag{37}$$

so that the likelihood ratio is given by

$$\Lambda(\boldsymbol{x}) = c\exp\big(R^d\boldsymbol{x}\Sigma^{-1}\boldsymbol{\mu}\big), \tag{38}$$

for some constant c independent of the data $\boldsymbol{x}$ and of the inclusion's parameters $(R, \mathbf{x}_b)$. The Neyman-Pearson lemma again asserts that Type II errors for a given Type I error are minimized for tests of the form (29).

Upon taking the log of the above likelihood ratio, we observe that these tests are equivalent to tests of the form $t = \boldsymbol{x}\Sigma^{-1}\boldsymbol{\mu} > \tau$. In other words, $t = t(\boldsymbol{x})$ is a *sufficient* statistic for the data. Moreover, we verify that

$$t \sim \mathcal{N}(0, \sigma_t^2), \qquad \text{where} \qquad \sigma_t^2 = \boldsymbol{\mu}\cdot\Sigma^{-1}\boldsymbol{\mu}. \tag{39}$$

Assuming that $\boldsymbol{\mu}$ is known, i.e., that $\mathbf{x}_b$ is known, we obtain a UMP test (optimal independent of the value of $R > 0$) as follows:

$$\begin{array}{lll} \text{Reject} & H_0 & \text{if} \quad t\big((-\delta\tilde{u}_m)_{1\leq m\leq M}\big) > \tau, \\ \text{Accept} & H_0 & \text{otherwise,} \end{array} \tag{40}$$

where

$$\alpha = \int_{t(\boldsymbol{x})>\tau} l_0(\boldsymbol{x})d\boldsymbol{x} = \int_{t>\tau} l_0(t)dt = 1 - \Phi\Big(\frac{\tau}{\sigma_t}\Big). \tag{41}$$

The above test is clearly optimal (uniformly most powerful) when the inclusion is at $\mathbf{x}_b$. However, in practice, the location $\mathbf{x}_b$ is not known and the test has to be modified. Since $\boldsymbol{\mu}$ is not available, we replace it by some $M-$vector $\boldsymbol{\mu}^R$ and define

$$t^R(\boldsymbol{x}) = \boldsymbol{x}\Sigma^{-1}\boldsymbol{\mu}^R \sim \mathcal{N}(0, (\sigma_t^R)^2), \quad \text{where} \quad (\sigma_t^R)^2 = \boldsymbol{\mu}^R \cdot \Sigma^{-1}\boldsymbol{\mu}^R. \tag{42}$$

For this new scalar data $t^R(\boldsymbol{x})$, we can now construct a UMP test consisting of rejecting H_0 when $t^R((-\delta\tilde{u}_m)_{1\leq m\leq M}) > \tau$, where

$$\alpha = 1 - \Phi\Big(\frac{\tau}{\sigma_t^R}\Big), \qquad 1-\beta = 1 - \Phi\Big(\frac{\tau - t^R}{\sigma_t^R}\Big). \tag{43}$$

How powerful the test will be depends on the accuracy of the estimate $\boldsymbol{\mu}^R$ with respect to $\boldsymbol{\mu}$. In practice, where one may expect to perform several measurements at locations $\mathbf{x}_m$ that are relatively close to each other (but still sufficiently far apart so that the measures are statistically independent), and far away from the inclusion $\mathbf{x}_b$, we can expect that $-\delta u(t, \mathbf{x}_m; R, \mathbf{x}_b)$ is almost independent of $\mathbf{x}_b$ and that $\sigma_m = \sigma$ is relatively close to a constant. In such an idealized case, $\boldsymbol{\mu}^R = (1, \ldots, 1)$ is quasi optimal and the level of confidence and the power of the statistical test are given by

$$\alpha = 1 - \Phi\Big(\frac{\tau}{\sqrt{M}\sigma}\Big), \qquad 1-\beta = 1 - \Phi\Big(\frac{\tau - t^R}{\sqrt{M}\sigma}\Big). \tag{44}$$

Not surprisingly, we observe that M measurements have the effect of increasing the signal-to-noise ratio by a factor $\sqrt{M}$.

All the above results can easily be generalized to arbitrary values of D_1. However the tests are based on whether $D_0 < D_1$ (the case considered here) or $D_0 > D_1$, in which case $\delta u > 0$, and therefore incorporate which type of inclusions one expects. For instance, $D_1 = 0$ corresponds to a perfectly reflecting inclusion characterized by Neumann boundary conditions at its boundary. As far as detection goes, the signal variation $u - u_0$ coming from such inclusions will be the exact opposite to the case $D_1 = \infty$ treated above as an example. When the sign of $D_0 - D_1$ is not known a priori, statistical tests may still be developed, however they will no longer be uniformly most powerful; we refer to [23].

6 Direct versus Time Reversal measurements

We have seen in the preceding section how to construct statistical tests to detect the presence of inclusion from diffusion measurements. We have also seen that the time reversal *filters* $F(t, \mathbf{x}, k)$ defined in (15) and the *direct* measurements $U(t, \mathbf{x}, k)$ defined in (20) both satisfied the same equation. The only difference in the equations is the choice of initial conditions namely, of the form $\chi(\mathbf{x})$ for F and $\delta(\mathbf{x} - \mathbf{x}_0)$ for U by appropriately choosing $\mathbf{S}(\mathbf{x})$. These initial conditions are qualitatively quite similar, and one could choose $\chi(\mathbf{x}) = \delta(\mathbf{x} - \mathbf{x}_0)$ (modeling an array of detectors small at the diffusive scale $\mathbf{x}$ but nonetheless large compared to the wavelength at the scale $\varepsilon\mathbf{x}$) so that $F(t, \mathbf{x}, k) = U(t, \mathbf{x}, k)$.

In such a context, the reconstruction of the inclusion from $U(t, \mathbf{x}, k)$ and from $F(t, \mathbf{x}, k)$ would give qualitatively quite similar results in the presence of very small

noise. Large differences between reconstructions from direct and from time reversal measurements are therefore to be looked for in regimes of large noise levels. We assume that t, $\mathbf{x}$, and k are fixed so that we have access only to one measurement to simplify namely, F in the time reversal framework and U in the direct framework. We also assume that U is the total energy measured on the array of detectors $\chi_\Omega(\mathbf{x})$. Note that the direct measurement U only requires us to measure the total energy at the detectors. In comparison, F requires us to measure the whole wave field on the detectors, time reverse it, and send it back into the media. The latter measurements thus necessitate a much more elaborate (and expensive) setting than the former.

Let us introduce the notation

$$\tilde{F} = F + n_{\mathrm{F}}, \qquad \tilde{U} = U + n_{\mathrm{U}}, \tag{45}$$

where $\tilde{F}$ and $\tilde{U}$ are the measured data. We now characterize the noise levels n_{F} and n_{U} and show that in some important practical situations, the signal to noise ratios $F/n_{\mathrm{F}} \gg U/n_{\mathrm{U}}$. We distinguish three types of noise:

- Noise n_{m}, with variance σ_{m}^2, caused on the diffusion solutions by the random fluctuations in the underlying media.
- Noise n_{d}, with variance σ_{d}^2, caused on the measured fields at the recording array (assumed additive to model background noise).
- Noise n_{f}, with variance σ_{f}^2, caused on the measured filter at the source location (assumed multiplicative to model detector defects).

The two last noises are classical and merely correspond to errors in the measured data. The first error models the accuracy of the diffusion approximation. Three mechanisms contribute to this error. Firstly, the asymptotic limit is derived in the limit $\varepsilon \to 0$ whereas ε is finite in practice. Secondly, the estimate on the background diffusion coefficient D_0 may not be perfect. Thirdly, the diffusion approximation may often be valid only for the statistical average (with respect to the realizations of the random media) of the energy density. The approximation may be valid independent of the realization only in cases of *statistical stability*. Several theories exist that show that macroscopic quantities such as the energy density of waves are statistically stable [8, 9, 39]. There are however situations in which the statistical stability does not hold even though the wave energy density solves on average a macroscopic equation [6]. Moreover, statistical stability can often be proved only in an integrated sense (see the references mentioned above). The statistical *instability* is modeled by σ_{m}^2. For want of a better model, we shall assume that all these errors are mean-zero Gaussian processes.

It remains to relate the variances σ_{m}^2, σ_{d}^2, and σ_{f}^2 to the noise levels n_{F} and n_{U}. Let $\mathbf{u}_\varepsilon(t, \mathbf{x})$ be the solution of (3) with initial condition such that $\hat{\mathbf{S}}(\mathbf{k})$ is supported on the sphere of modulus k. This is how the filters F and the direct measurements U are constructed. At times t of order $O(1)$, the energy recorder at the array of detectors $\chi_\Omega(\mathbf{x})$ will be of order $O(1)$, i.e., a fraction of the initial energy. The signal at the array of detectors will be

$$\tilde{\mathbf{u}}_\varepsilon(t, \mathbf{x}) = \mathbf{u}_\varepsilon(t, \mathbf{x}) + \mathbf{n}_{\mathrm{d}}(\mathbf{x}). \tag{46}$$

We assume that the noise distribution is independent of the solution $\mathbf{u}_\varepsilon$, which is quite reasonable in practice if $\mathbf{n}_\mathrm{d}$ models a background noise. Further assuming that $\mathbf{n}_\mathrm{d}(\mathbf{x})$ and $\mathbf{n}_\mathrm{d}(\mathbf{y})$ for two different detectors at $\mathbf{y} \neq \mathbf{x}$ are uncorrelated to simplify, and that the number of detector in the array is large so that the law of large numbers applies, we obtain

$$\tilde{U} = (1 + n_\mathrm{m})U + \sigma^2_\mathrm{ad}, \qquad \sigma^2_\mathrm{ad} = \int_{\mathbb{R}^3} \chi^2(\mathbf{x}) \frac{1}{2} \mathbb{E}\big\{ \mathbf{n}_\mathrm{d}(\mathbf{x}) \cdot A(\mathbf{x}) \mathbf{n}_\mathrm{d}(\mathbf{x}) \big\} d\mathbf{x}. \tag{47}$$

In other words, the direct energy measurements consist of the sum of the energy of the true signal and the energy of the background noise since both signals are uncorrelated. We recall that U is the exact solution of the diffusion approximation and that $n_\mathrm{m}U$ models the accuracy of that diffusion approximation. This is the model for the direct measurements. We observe that $\tilde{U}$ is a biased estimate of U. In practice, we may be able to estimate the variance σ^2_ad, for instance by probing the background noise level before starting the measurements. We may for instance assume that

$$\sigma^2_\mathrm{ad} = \bar{\sigma}^2_\mathrm{ad} + n_\mathrm{de},$$

where $\bar{\sigma}^2_\mathrm{ad}$ is known and n_de is a mean zero Gaussian variable with variance σ^2_de. Then $\tilde{U} - \bar{\sigma}^2_\mathrm{ad}$ becomes an unbiased estimate for U with law $\mathcal{N}(0, \sigma^2_\mathrm{de})$.

Let us now consider the time reversal measurement $\tilde{F}$. The filter is obtained by backpropagating the measured signal in (46) for a duration t. The noise signal $\mathbf{n}_\mathrm{d}(\mathbf{x})$ has amplitude and energy of order $O(1)$ and is not correlated to the true signal $\mathbf{u}_\varepsilon(t, \mathbf{x})$. Its amplitude will therefore remain of order $O(1)$ after back-propagation. In contrast, the true signal $\mathbf{u}_\varepsilon(t, \mathbf{x})$ will backpropagate to give a signal of order $F\varepsilon^{-3/2}\hat{\mathbf{S}}$ according to (13), i.e., of order $\varepsilon^{-3/2}$ in the vicinity of $\mathbf{x}_0$. We can thus model the measured filter as

$$\tilde{F} = (1 + n_\mathrm{f} + n_\mathrm{m})F + \varepsilon^{3/2} n_\mathrm{md}, \tag{48}$$

where n_md is obtained by backpropagating $\mathbf{n}_\mathrm{d}(\mathbf{x})$ through the random media for a duration t and dividing by $\hat{\mathbf{S}}(\mathbf{k})$ as in (17). Thanks to the powerful refocusing property of time reversed waves, the amplitude of the back-propagated measured signal is of order $\varepsilon^{-3/2}$. This implies that the signal-to-noise ratio $F/n_\mathrm{md} \sim \varepsilon^{-3/2}$, which renders legitimate the assumption that the errors performed in the measurements are multiplicative rather than additive, whence the multiplicative noise n_f.

We have modeled unbiased estimates for U and F based on noise scenarios, which we believe are realistic, at least qualitatively. In order to test for the presence of an inclusion, we can now subtract the solution U_0 and F_0 obtained by solving the diffusion equations in a homogeneous known background. We thus obtain

$$\begin{array}{rcccl} \delta\tilde{U} & = & \tilde{U} - \bar{\sigma}^2_\mathrm{ad} - U_0 & = & \delta U + n_\mathrm{m}U + n_\mathrm{de} \\ \delta\tilde{F} & = & \tilde{F} - F_0 & = & \delta F + (n_\mathrm{f} + n_\mathrm{m})F + \varepsilon^{3/2} n_\mathrm{md}. \end{array} \tag{49}$$

Thus $\delta\tilde{U}$ and $\delta\tilde{F}$ are both unbiased estimates of $\delta U = U - U_0$ and $\delta F = F - F_0$, respectively. The main difference is how the detector noise $\mathbf{n}_\mathrm{d}$ is handled.

In practice, where the distance between the object and the detectors is sufficiently large, we may expect the energy level at the detectors to be quite small. It is then not

unrealistic to assume that $n_{\rm de}$, even after suitable filtering, is comparable to the signal δU. The signal to noise ratio $\delta U/n_{\rm de}$ may then be too faint to allow for good detection capabilities, as the test (31) shows. In contrast, the signal to noise ratio $\delta F/(\varepsilon^{3/2} n_{\rm md})$ is quite large, and it is likely that the detection limit will be caused by errors in the model $n_{\rm m} F > \varepsilon^{3/2} n_{\rm md}$, or by errors in the measurements of the refocused signal $n_{\rm f} F > \varepsilon^{3/2} n_{\rm md}$.

7 Reconstructing the inclusion

Once an inclusion has been detected, one may want to obtain additional information. In the model proposed in this paper, the reconstruction consists of identifying the diffusion coefficient from measurements of the diffusion solution at different locations $\mathbf{x}$ and times t. Although the full diffusion coefficient may be identifiable from a reasonably large set of measurements [34, 36], the problem is severely ill-posed so that even small errors in the measured data may have drastic consequences on the reconstruction.

Here we assume that the asymptotic expansion (22) holds and that the remainder may be neglected. The Green function and the solution $u_0(T, \mathbf{x})$ are those of an infinite homogeneous medium. We also assume that $D_1 = +\infty$ and that $D_0 = 23$ as in the previous numerical simulations. There are therefore $d + 1$ parameters to reconstruct namely, $\mathbf{x}_b = (90, 50)$ (in arbitrary units) and R. We consider the two-dimensional configuration $d = 2$ and assume that we have access to four measurements. Because the inverse problem has been simplified so as to involve only a finite number of parameters, the reconstruction becomes stable, in the sense that noise in the data is not amplified during the reconstruction by more than a constant [2, 5]. We have performed some

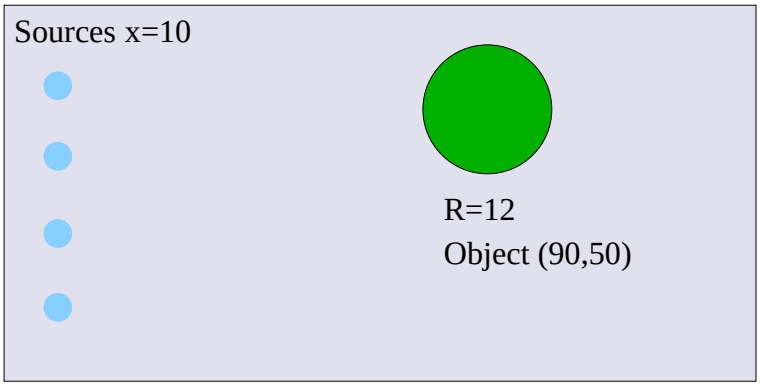

Figure 2: Geometry for the reconstruction of inclusions from noisy measurements $\delta\tilde{u}$ based on fluctuations δu given by the leading term in (22) and Gaussian multiplicative noise (see text).

numerical reconstructions from synthetic diffusion data based on the formula (22). The geometry is presented in Fig. 2 and is similar to one of the cases treated in Fig. 1. We consider a configuration with four measurements in the echo-mode all situated on one side of the domain, which corresponds to situations encountered in practice. The background $u_0(250, \mathbf{x})$ is evaluated at $T = 250$ and at the four source locations (where detectors are also located). In this configuration, $\delta u(250, \mathbf{x})$ given by the leading term in (22) is roughly 1.8% of $u_0(250, \mathbf{x})$ for the inclusion depicted in Fig. 2, whereas the time

maximizing $\delta u(\cdot, \mathbf{x})/u_0(\cdot, \mathbf{x})$ is $T = 200$. A background mean-zero Gaussian noise n_n of variance $\sigma_{\rm n}^2 = (ku_0)^2$ is added to the data $\delta\tilde{u} = \delta u + n_n$, where $k = 0.25\%, 0.5\%, 1\%$. The best fit to the data given by (22) is calculated by least-square minimization. The standard deviation of the reconstructed characteristics of the inclusion (x_b, y_b, R) is estimated from 10 realizations of the random noise and displayed in Tab. 1. The errors

$\sigma_{\rm n}/u_0$	error on R (%)	error on x_b (arb. units)	error on y_b (arb. units)
0.25%	12	9.0	3.5
0.5%	25	15	5.0
1%	33	30	10

Table 1: Error in the reconstruction of the characteristics of inclusions (radius R and position $\mathbf{x}_b = (x_b, y_b)$) in the setting of Fig. 2. An error of order 0.25% for $\delta u/u_0$ corresponds to an error of order 15% for δu.

on the location and volume of the inclusion (the error on the volume R^2 is roughly twice that on R) should grow linearly with the noise level, which is roughly observed in the data.

Let us conclude this section with a few remarks. Firstly, the cost function used in the minimization has many local minima. A Newton-type technique will thus converge to the global minimum only if the initial estimate is sufficiently accurate. Global minimization algorithms are thus necessary. Secondly, although the noise level is indeed small compared to the measurements $u(T, \mathbf{x})$, it is already relatively large compared to the signal $\delta u(T, \mathbf{x})$. Quite accurate measurements are therefore necessary to obtain good reconstruction capabilities. An error of order 1% on four detectors that are relatively closely spaced as in Fig. 2 correspond to an error of order 0.5% if we had only one detector (assuming that noise at the four detectors is uncorrelated). In the ROC curves presented in Fig. 1, we see that an error of order 0.5% gives very good detection probabilities (the probability of missed detection is $\beta = 3\,10^{-4}$ for a probability of false alarm $\alpha = 0.05$). Yet the errors on the reconstructions for $k = 1\%$ are quite large. Much more accurate data are required to reconstruct the inclusion than to simply detect it. Finally, we see in Tab. 1 that the cross-range reconstructions (y_b) are better than the range reconstructions (x_b), which is classical (and obvious) in the geometry of Fig. 2. It is substantially better because of the larger aperture of the chosen array of measurements.

8 Acoustic wave simulation

The preceding sections were concerned with an analysis of the detection and imaging capabilities of time reversal techniques when the energy density of waves is modeled by a macroscopic diffusion equation. The theory could be modified to accommodate various macroscopic regimes for the energy density, such as radiative transfer [11, 40], Fokker-Planck [8] or a paraxial approximation [9, 16, 39]. A fundamental property in all these models is the *statistical stability* of the wave energy density. Indeed, in situations where only a few measurements may be performed, it is important that they depend

as little as possible on the realization of the underlying media and rather only on its statistical properties.

The objective of this section and the next section are precisely to verify this statistical stability numerically. The main challenge numerically is that wave propagation should occur over a domain very large compared to the typical wavelength in the system. Moreover the random media need to be carefully simulated so that prescribed statistical properties are satisfied. Once this is achieved, we need to demonstrate that the regime of radiative transfer, and then its diffusion approximation, are good models for the wave energy density.

This section describes the numerical setting and the validity of the macroscopic model for the wave energy density. The next section addresses the question of the statistical stability of different types of measurements and considers the detection capabilities of time reversal techniques in such synthetic environments.

Computational setting. We discretize the first-order hyperbolic system (1) for pressure $p(t, \mathbf{x})$ and velocity $\mathbf{v}(t, \mathbf{x})$ augmented with suitable initial conditions and surrounded by a perfectly matched layer [14, 15] by finite element method [21]. This yields the discrete linear system

$$M_V \frac{d\mathbf{V}}{dt} = R^t P, \qquad M_P \frac{dP}{dt} = -R\mathbf{V}, \tag{50}$$

for the discrete pressure P and velocity $\mathbf{V}$. By appropriate mass lumping [21] both mass matrices M_P and M_V are diagonal and the scheme is second-order accurate.

In all our simulations, we assume that

$$\rho = 1, \qquad \kappa(\mathbf{x}) = 1 + \sqrt{\varepsilon}\kappa_1\Big(\frac{\mathbf{x}}{\varepsilon}\Big), \tag{51}$$

where κ_1 is a stationary mean-zero random variable. The effective sound speed in thus $c_0 = 1$. The fluctuations are characterized by the two-point correlation function

$$R(\mathbf{x}) = \mathbb{E}\{\kappa_1(\mathbf{x}+\mathbf{y})\kappa_1(\mathbf{x})\},$$

and by their power spectrum $\hat{R}(\mathbf{k})$, the Fourier transform of $R(\mathbf{x})$. The fluctuations of the compressibility $\kappa_1(\mathbf{y})$ have been carefully modeled to verify prescribed power spectra as in [13]. When we say that the media have fluctuations of order $x\%$, we refer to the standard deviation of κ_1 (with respect to $\kappa_0 \equiv 1$).

The theory of time reversed waves in diffusive regimes was summarized in (13). The source terms need to be localized in the vicinity of a point $\mathbf{x}_0$ and at the same time have an oscillatory behavior at the frequency $\mathbf{k}/\varepsilon$ (reduced frequency $\mathbf{k}$). In the simulations, the localized source term at wavenumber $\mathbf{k}_0$ is chosen of the form

$$\mathbf{S}(\mathbf{x}) = \left(\mathbf{0}, \exp\left(\frac{-|\mathbf{x}-\mathbf{x}_0|^2}{2\sigma^2}\right)\cos(\mathbf{k}_0\cdot\mathbf{x})\right)^t. \tag{52}$$

Typically σ is on the order of 5 wavelengths $\lambda_0 = 2\pi/|\mathbf{k}_0|$ so that the frequency content of $\mathbf{S}$ is primarily that of a single (standing) planewave. When we talk about the typical wavelength in the system, we refer to that specific λ_0. The simulations are performed

using on the order of 13 grid points per wavelength and are two-dimensional. Once the simulations are run, the filters are calculated according to (17). In all our simulations, the array of detectors is a rectangle whose boundary has been smoothed out ($\chi_\Omega(\mathbf{x})$ is a regularized version of the characteristic function on the rectangle) to avoid spurious numerical oscillations.

Transport and diffusion equations. The transport (or radiative transfer) regime is characterized by knowledge of a transport mean free path $\Sigma^{-1}(k)$, which is also here a transport mean free time since $c_0 \equiv 1$. The transport mean free path roughly indicates the mean distance between successive interactions of the wave energy density with the underlying media. $\Sigma(k)$ is also called the total scattering coefficient.

The transport mean free path can be related to the power spectrum $\hat{R}(\mathbf{k})$ of the compressibility fluctuations as follows. In our numerical simulations, the power spectrum is chosen as

$$\hat{R}(k) = \hat{R}_0 \begin{cases} 1 & \text{for} \quad k < M \\ 0 & \text{for} \quad k > M. \end{cases} \tag{53}$$

The value M is chosen slightly larger than the wavenumbers k_0 in the system so as to maximize interaction between the waves and the underlying fluctuations. In the simulations, we use the adimensionalized values $k_0 \approx 6.28$ (corresponding to $\lambda_0 = 1$ precisely) and $M \approx 8.08$. In two space dimensions, we obtain [40] that

$$\Sigma(k) = \frac{k^3 \hat{R}_0}{4\pi} \begin{cases} \pi & \text{for} \quad k < \dfrac{M}{2} \\ \arccos\left(1 - \dfrac{M^2}{2k^2}\right) & \text{for} \quad k > \dfrac{M}{2}. \end{cases} \tag{54}$$

We now want to estimate the transport mean free path numerically. It turns out that $\Sigma^{-1}(k)$ also indicates how the coherent energy (coherent with respect to the initial source term) in the system decays as a function of time. Let $\mathbf{u}(t, \mathbf{x})$ be the solution of the hyperbolic system (1) in heterogeneous media, $\mathbf{u}_{\mathrm{H}}(t, \mathbf{x})$ the same solution in a homogeneous domain, and $\mathcal{E}(t, \mathbf{x})$ and $\mathcal{E}_H(t, \mathbf{x})$ the corresponding energies defined in (18). It is then well-known that the coherent energy decays exponentially [35] so that we have approximately

$$\frac{(\mathcal{E}(t,\cdot), \mathcal{E}_{\mathrm{H}}(t,\cdot))}{(\mathcal{E}_{\mathrm{H}}(t,\cdot), \mathcal{E}_{\mathrm{H}}(t,\cdot))} = e^{-\Sigma(k_0)t}, \tag{55}$$

at least in the limit of high frequencies. We recall that the speed $c_0 \equiv 1$. Here $k_0 = |\mathbf{k}_0|$ is the wavenumber of the source term. This is the test we use to estimate Σ numerically and compare it to the theoretical prediction (54). The log of left- (right-) hand side in (55) is estimated numerically (theoretically) in Fig. 3. We observe a very good qualitative agreement between the numerical simulation and the theoretical prediction. Notice that for an object about 100 wavelengths apart from the source in a media with 8% fluctuations, the signal will travel at least six transport mean free paths before reaching the detectors (also at the source location). The coherent signal will thus be about one part in a thousand of the original signal and is likely to be too faint to be useful in practical detections. Based on knowledge of the transport mean free path, we can estimate the diffusion coefficient according to the formula:

$$D(k) = \frac{1}{2(\Sigma(k) - \lambda(k))}, \tag{56}$$

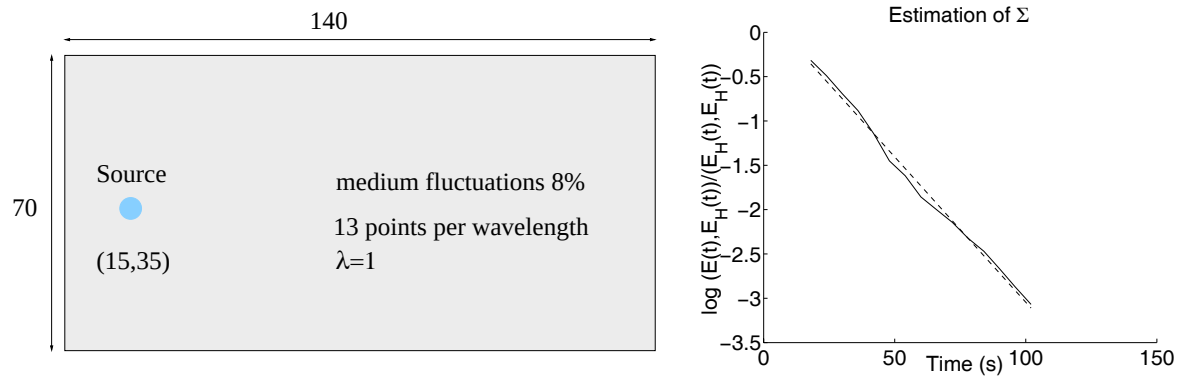

Figure 3: Left: geometry of the simulation (surrounded by a perfectly matched layer). Right: theoretical and numerical estimation of Σ. In media with 8% fluctuations, the theoretical value of Σ based on (54) is $\Sigma_{\rm th} = 0.0338$. The estimated value through (55)) is $\Sigma_{\rm num} = 0.0328$. The curve presents the log of normalized correlation defined in (55). The solid line is the left-hand side and the dotted line $-\Sigma_{\rm th} t$.

in two space dimensions, where

$$\lambda(k) = \frac{1}{4\pi} k^3 \begin{cases} 0 & \text{for} \quad k < M/2, \\ \dfrac{\hat{R}_0\, M}{2\, k} \Big(1 - \dfrac{M^2}{4k^2}\Big)^{1/2} & \text{for} \quad k > M/2. \end{cases} \tag{57}$$

Based on the numerical and theoretical estimates for Σ, we find for $D(k)$ the values 23.64 and 22.87, respectively. The *mean free path* $(\Sigma(k) - \lambda(k))^{-1} = 2D(k) \geq \Sigma^{-1}(k)$ is a good indication of the distance that waves need to travel before a significant change of direction may be observed because of scattering effects. Its numerical value is roughly 46 in our experiments compared to 30 for the transport mean free path.

A direct numerical evaluation of the diffusion coefficient (without using the formula (56)) would be much more satisfactory as it would not rely on knowing the specific shape of the power spectrum. This is however a much more difficult task as waves need to propagate for quite a few mean free times before they can reach the diffusive regime. An additional complication in bounded domains arises with the boundary conditions one has to impose to the diffusion equation. It is well known that appropriate boundary conditions to model escape of energy at the domain boundary (through the perfectly matched layer in our simulations) are of the form [7, 22]

$$U + 2LD \frac{\partial U}{\partial \boldsymbol{\nu}} = 0, \tag{58}$$

where L is an extrapolation length and $\boldsymbol{\nu}$ the normal unit vector at the boundary of the domain.

We have fitted the diffusion solution with the above boundary conditions to the time reversal filters for the geometry presented in Fig. 6 in the next paragraph (reproduced on the left picture in Fig. 4) and for an initial condition of Bessel type given in (59). Initial conditions of the form (59) are much better than (52) because of their directional independence. Note however that most of the signal has frequency $k_0 = |\mathbf{k}_0|$ and is thus expected to diffuse according to the diffusion coefficient $D(k_0)$. The numerical fit for the

diffusion coefficient and the extrapolation length L in (58) was based on measurements of the filters and of the diffusion approximation for times between $T_1 = 220$ and $T_2 = 270$. This corresponds to a propagation of roughly $4 - 5$ mean free paths (defined as $2D$). The time reversal filters calculated from the wave simulations and the diffusion approximation are presented in Fig. 4. The results of the best fit are $D_{\rm num} = 26.56$

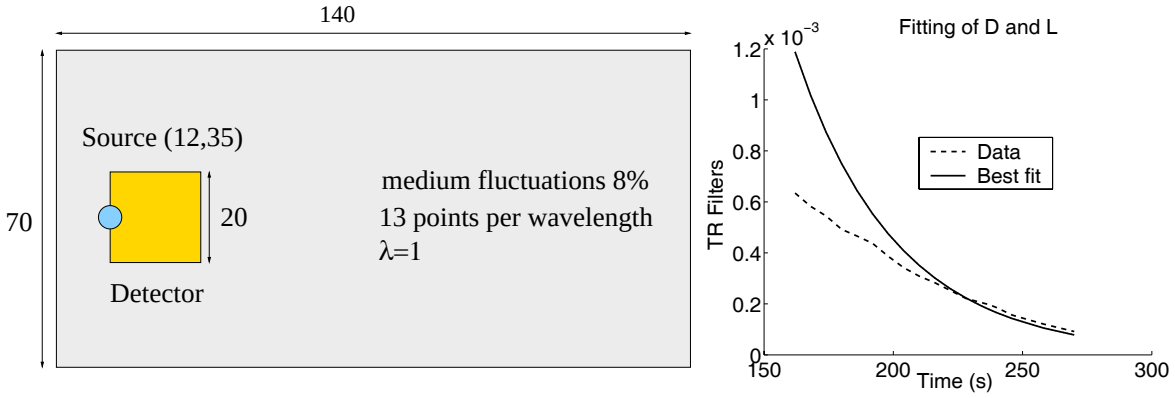

Figure 4: Right: Comparison between the time reversal filters obtained from wave calculations in the geometry the left picture and the diffusion approximation.

(whereas the exact coefficient is $D_0 \approx 23$) and $L_{\rm num} = 1.12$. Although the reconstruction is not nearly as accurate as for Σ, we were still able to obtain a reasonable value for the diffusion coefficient. Further numerical simulations in much larger domains are necessary to address the reconstruction of diffusion coefficients in random media.

9 Stability and Statistical tests

The preceding section showed how the main characteristics of the transport and diffusive regimes, namely $\Sigma(k)$ and $D(k)$ could be estimated numerically from simulation of waves in highly heterogeneous media. The successful detection and imaging of inclusions from time reversal data presented in earlier sections hinges on one major assumptions namely, that the noise level $n_{\rm m}$ is smaller than the fluctuation caused by the presence of the object. Smallness of $n_{\rm m}$ follows from: (i) we can assess the statistical properties of the random media with sufficient accuracy; (ii) the macroscopic solution is sufficiently stable statistically, in the sense that it does not depend too largely on the realization of the random media with prescribed statistics.

The preceding section dealt with (i). We now address (ii), which to a large extent we believe is the most important impediment to successful detection from time reversal measurements. Indeed, whereas background noise can significantly be reduced by time reversal measurements ($n_{\rm d}$ is replaced by $\varepsilon^{d/2} n_{\rm d}$ in d space dimensions), detection and imaging eventually require a stable model for the measured macroscopic quantity (the filters). Errors in the model for the measurements, including their statistical stability, strongly correlate with detection and imaging capabilities as we have seen in sections 5 and 7.

Many macroscopic models for wave propagation in random media enjoy statistical stability properties [8, 9, 39], though statistical stability is not always ensured [4, 6,

41], for instance because of localization effects or because very singular objects are considered. Even when statistical stability is ensured, it holds for various averaged (integrated) quantities (see the references mentioned above) and not point-wise in $\mathbf{x}$ and k for the filter $F(t, \mathbf{x}, k)$. The question should therefore be raised in a slightly different context. What one should ask is how much the specific measurement (possibly averaged) we have at our disposal is statistically stable based on what we know about the random media.

Stability of the Filters. In order to gain stability in the measurements, we construct a source term whose wavenumber content is localized in $k = |\mathbf{k}| \in \mathbb{R}^+$ rather that $\mathbf{k} \in \mathbb{R}^2$ (the simulations are performed in two-space dimensions). Such a source takes the form of a localized Bessel function spatially localized by a Gaussian envelope. More precisely, we choose

$$p_0(\mathbf{x}) = J_0\left(|\mathbf{k}_0||\mathbf{x} - \mathbf{x}_0|\right) \exp\left(-\frac{|\mathbf{x} - \mathbf{x}_0|^2}{2\sigma^2}\right), \tag{59}$$

where J_0 is the zero-th order Bessel function of the first kind and $\sigma = 3$. The initial velocity $\mathbf{v}(0, \mathbf{x})$ is set to $\mathbf{0}$. Because the initial condition is highly peaked for wavenumbers such that $|\mathbf{k}| = k$, we verify that (17) can be approximated by

$$F(t, \mathbf{x}_0, |\mathbf{k}_0|) = \frac{1}{2\pi} \int_{S^1} \frac{\hat{\mathbf{u}}^B(|\mathbf{k}_0|\hat{\mathbf{k}})}{\hat{\mathbf{u}}_0(|\mathbf{k}_0|\hat{\mathbf{k}})} d\hat{\mathbf{k}}. \tag{60}$$

Here $\mathbf{u}_0(\mathbf{x}) = \mathbf{u}(0, \mathbf{x})$ the initial source term. Numerically the filters are obtained by taking the ratios of the pressure fields (the third component of the vector $\hat{\mathbf{u}}(\mathbf{k})$ in two space dimensions) and approximating the above integral. We consider the configuration of the simulation described in Fig. 5. We have considered two sizes for the array of

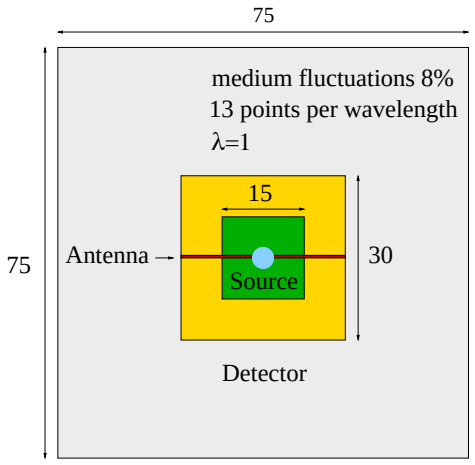

Figure 5: Numerical setting to assess the stability of the filters.

detectors 15×15 and 30×30 wavelengths recording the signal at $T = 160$, and an antenna of size 30 wavelengths recording a signal between times $T = 120$ and $T = 160$ (a time span of 40 periods since $c_0 = 1$). In all configurations, the filters are calculated for an initial condition of the cosine type as in (52) and for an initial condition of the Bessel type as in (59). The simulations were performed with 16 different realizations

of the random media characterized by the power spectrum described in (53) in which $\hat{R}_0 = 0.08$. Since $(\Sigma(k) - \lambda(k))^{-1} \approx 45$, a simulation with $T = 160$ corresponds to waves propagating for roughly 4 mean free paths before time reversal, which is already significant. The standard deviation of the filters in (60) has been estimated for each configuration. The results are presented in Tab. 2.

	Bessel			Cosine		
Detection	30×30	15×15	Antenna	30×30	15×15	Antenna
STD (%)	4.6	6.8	4.6	5.9	6.6	6.1

Table 2: Statistical stability of the measured signals after time reversal in several configurations; see text.

In the above simulations, we indeed observe a relatively good statistical stability of the filters (on the order of a few percents) that should provide us with reasonable detection capabilities for sufficiently large inclusions. This behavior depends however very much on the size of the array of detectors and on the frequency content of the initial condition.

Detection based on simulated data. The (relative) statistical stability demonstrated in the previous paragraph is independent of macroscopic models that the filters may or may not satisfy and is a prerequisite to imaging in media whose exact Green function is not known.

Let us now consider the geometry presented in Fig. 6. In all simulations, the media

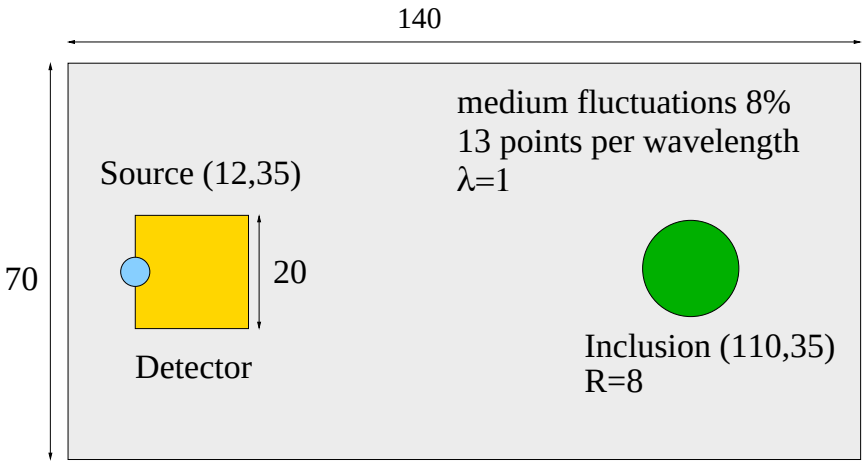

Figure 6: Geometry of the detection problem in the numerical simulations.

fluctuations are 8% and the initial condition is the Bessel function in (59). We have estimated the variation of the filters caused by inclusions located as in Fig. 6 and with radius between $R = 3$ and $R = 8$ for a duration of time reversal experiment $T = 160$. The filter variations as a function of inclusion's radius should scale as R^2 according to (22). We have observed numerically a variation of the form $R^{1.91}$, in quite good

agreement with theory, although many macroscopic models share a scaling in R^2 for the measurement variations.

For a radius $R = 8$ as in Fig. 6, we have numerically computed the time reversal filters and the direct energy measurements for various experiment durations T. Fig. 7 shows the total energy $U(T)$ measured at the array of detectors as a function of time. Three energies are presented: $U_0(T)$ in the absence of inclusion, $U(T)$ in the presence of the inclusion, and $\tilde{U}(T)$ in the presence of an inclusion and of noise modeled as in (47) with $n_{\rm m} = 0$ and $n_{\rm d}$ in (46) a mean-zero Gaussian variable with standard deviation $\sigma_{\rm d} = 7\%\|\mathbf{u}(T,\cdot)\|_{L^\infty}$ added to the measured field $\mathbf{u}(T,\cdot)$ at the array of detectors. We

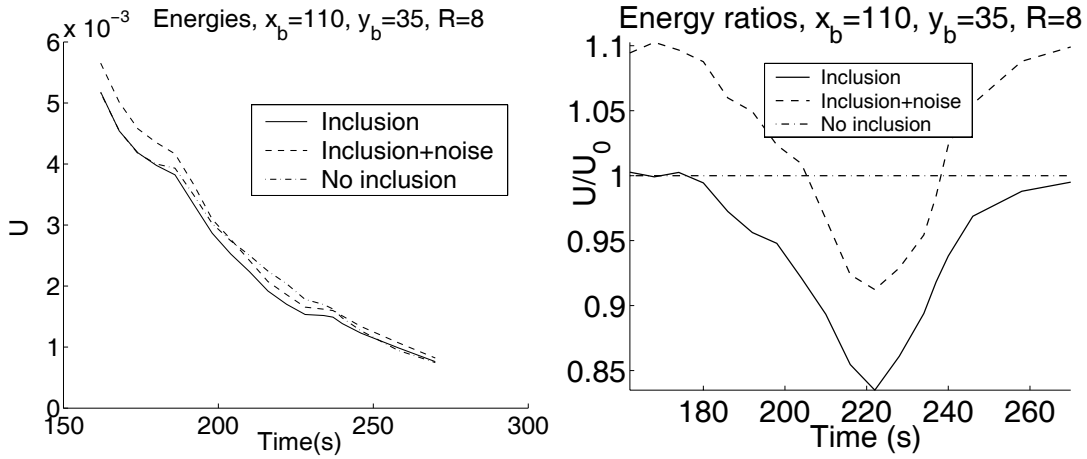

Figure 7: Left: Energies $U_0(T)$ (no inclusion; dash-dotted line), $U(T)$ (inclusion, no noise; solid line) and $\tilde{U}(T)$ (inclusion with noise; dotted line) for different values of T in the configuration presented in Fig. 6. Right: Energy ratios; same energies divided by $U_0(T)$.

have not tried to remove the energy $\bar{\sigma}^2_{\rm ad}$ from the unbiased estimate $\tilde{U}$ of U. Note that in such a configuration, the noise level is such that it renders detection of the object impossible since the error $\tilde{U} - U$ is comparable or in size to $U - U_0$. Since we have chosen the variance of the noise to be a constant percentile of $U_0(T)$ (for illustration purposes only as this is unlikely to happen in practice), filtering such a component out of the data may be relatively easy. However background noise with more complicated unknown time dependence may be more difficult to handle.

Time reversal measurements are immune to such noise. We present in Fig. 8 the filters measured in the same configuration of Fig. 6. Filters are evaluated at the source location $\mathbf{x}_0$ and for the wavenumber $|\mathbf{k}_0|$. As for direct measurements, three filters are presented: $F_0(T)$ in the absence of inclusion, $F(T)$ in the presence of the inclusion, and $\tilde{F}(T)$ in the presence of an inclusion and of noise modeled as in (47) with $n_{\rm m} = 0$ and $n_{\rm d}$ in (46) a mean-zero Gaussian variable with standard deviation $\sigma_{\rm d} = 100\%\|\mathbf{u}(T,\cdot)\|_{L^\infty}$ added to the measured field $\mathbf{u}(T,\cdot)$ at the array of detectors. We observe that the added background noise added at the level of the detectors has a minor influence on the filters. A noise of standard deviation roughly 15 times higher than for the direct measurements $\tilde{U}(T)$ barely modifies the filters (since $\tilde{F}(T) - F(T)$ is less that one percent of $F_0(T)$) and much smaller than the fluctuations $n_{\rm m}F_0(T)$ expected from the statistical instability of the medium (on the order of five percent of $F_0(T)$ for the simulations presented in

Tab. 2).

In the absence of background noise, both the direct measurements $U(T)$ and the time reversal measurements $F(T)$ offer the same detection and imaging capabilities. The variation of measurements reach 15% of the inclusion-free measurement for $T = 220$. Provided that the error due to statistical instability is 5% to fix ideas, this gives us a probability of detection $1 - \beta = 0.99$ for $\alpha = 0.05$ based on the statistical tests developed in section 5. For variations of order 10% and 5% (obtained at sub-optimal times), the probabilities of detection drop to 0.88 and 0.41, respectively. When statistical instability increases to 10%, the three probabilities of detection become 0.68, 0.41, and 0.17, respectively. Filters calculated by time averages as in (8) also need to be modified accordingly. Notice that estimating the maximum of $U(T)$ (provided that the background noise is sufficiently small so that $U(T)$ can be estimated) is simple: we just have to observe the measured intensity as a function of time. Estimating the maximum of $F(T)$ is a much harder problem as the filters at each duration T correspond to a totally different time reversal experiment. Time reversal thus offers a very powerful technique to eliminate the effect of background noise in the measurements, but its utilization is more delicate than that of direct energy measurements.

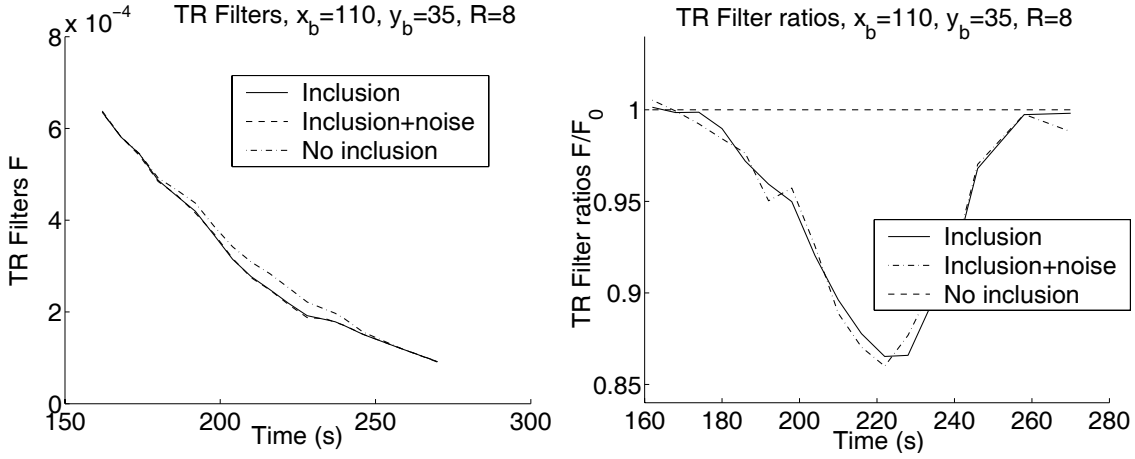

Figure 8: Left: Filters (modeled by (60)) $F_0(T)$ (no inclusion; dash-dotted line); $F(T)$ (inclusion, no noise; solid line) and $\tilde{F}(T)$ (inclusion with noise; dotted line) for different values of T in the configuration presented in Fig. 6. Right: Filter ratios; same filters divided by $F_0(T)$.

Let us conclude this section by a remark on the variations δF obtained in Fig. 8. Although the diffusion approximation was a sufficiently accurate representation of our numerical simulations to provide a reasonable fit for the diffusion coefficient in Fig. 4, it fails to give any accurate results for the variations δF in the geometry of Fig. 6. There are several explanations for why we should not expect diffusion to work. First of all, the variations in Fig. 8 are of order roughly similar to the variations expected from having an inclusion. The main reason is however the following: the models (21)-(22) assume that the fluctuations are much larger than the mean-free path in order for the diffusion approximation to hold. Even though the inclusion in Fig. 6 is large compared to the wavelength, it is small compared to the mean free path (on the order of 45 wavelengths). The fluctuations should thus not expect to follow a diffusive model (22) in this situation.

A more refined model of time reversal based on the equations of radiative transfer [11] is what we believe will give us the right macroscopic model for the curves observed in Fig. 8. This will be investigated in subsequent studies.

10 Conclusions

We have analyzed the detection and imaging of inclusions buried in highly heterogeneous media where the energy density of waves may be modeled by a diffusion equation. In this model, the inclusions are modeled as local fluctuations of the diffusion coefficient and must therefore typically be large compared to the wavelength of the waves used to probe them. Provided that the diffusive model is reasonably accurate and that the diffusion measurements are sufficiently stable statistically, we have developed statistical tests towards detection of the inclusion and asymptotic models to image the inclusions. We have demonstrated that time reversed waves, thanks to their enhanced refocusing properties, could efficiently be used even in the presence of strong background noise levels that would hamper the use of direct diffusion measurements to detect the buried inclusions. In the regime of interest in this paper, the media are also too heterogeneous for imaging techniques based on coherent signals and travel time measurements, for instance, to be efficient.

Unlike imaging methods based on wave propagation, the reconstructions proposed here rely on the availability of a macroscopic model and on the statistical stability of the measured data. Although detection and imaging becomes problem dependent, this is in our opinion the price to pay when the random media is not known exactly but rather only in a macroscopic statistical sense. We have insisted on the diffusion model in this paper for expository reasons. Very similar theories can be developed in other statistically stable macroscopic models, such as for instance models based on radiative transfer equations, which we plan to investigate further in the future. No matter what macroscopic model is retained, it is very likely that noise in the data (coming from approximate knowledge of the macroscopic model as well as from statistical instabilities) will be quite large. In such situations, imaging based on asymptotic expansions in the size of the inclusion provide powerful tools to understand which characteristics of the inclusions may or may not be reconstructed from data with a given noise level.

Further numerical and experimental studies are certainly necessary to assess the practical quality and validity of the imaging techniques proposed in this paper. This is the object of ongoing research by us and other groups.

Acknowledgment

We would like to thank Lenya Ryzhik and Chrysoula Tsogka for numerous discussions on time reversal. The wave propagation code used in the simulations was written in c++ and relies extensively on the library Getfem++ developed by Yves Renard and Julien Pommier. We would like to thank them for their generous technical support. The numerical simulations were performed on a LINUX cluster at Columbia University. This work was supported in part by DARPA-ONR grant N00014-04-1-0224. GB acknowledges support from NSF Grants DMS-0239097 and an Alfred P. Sloan Fellowship.

OP acknowledges support from an INRIA postdoctoral fellowship.

References

[1] D. G. Alfaro Vigo, J.-P. Fouque, J. Garnier, and A. Nachbin, *Robustness of time reversal for waves in time-dependent random media*, Stochastic Process. Appl., 113 (2004), pp. 289–313.

[2] H. Ammari, S. Moskow, and M. S. Vogelius, *Boundary integral formulae for the reconstruction of electric and electromagnetic inhomogeneities of small volume*, ESAIM Control Optim. Calc. Var., 9 (2003), pp. 49–66.

[3] K. Ammari and H. Kang, *Reconstruction of Small Inhomogeneities from Boundary Measurements*, Lecture Notes in Mathematics, Springer, Berlin, 2004.

[4] M. Asch, W. Kohler, G. Papanicolaou, M. Postel, and B. White, *Frequency content of randomly scattered signals*, SIAM Rev., 33(4) (1991), pp. 519–625.

[5] G. Bal, *Optical tomography for small volume absorbing inclusions*, Inverse Problems, 19 (2003), pp. 371–386.

[6] ——, *On the self-averaging of wave energy in random media*, SIAM Mult. Mod. Simul., 2(3) (2004), pp. 398–420.

[7] G. Bal, V. Freilikher, G. Papanicolaou, and L. Ryzhik, *Wave Transport along Surfaces with Random Impedance*, Phys. Rev. B, 62(10) (2000), pp. 6228–6240.

[8] G. Bal, T. Komorowski, and L. Ryzhik, *Self-averaging of Wigner transforms in random media*, Comm. Math. Phys., 242(1-2) (2003), pp. 81–135.

[9] G. Bal, G. Papanicolaou, and L. Ryzhik, *Self-averaging in time reversal for the parabolic wave equation*, Stochastics and Dynamics, 4 (2002), pp. 507–531.

[10] G. Bal and L. Ryzhik, *Time Reversal for Classical Waves in Random Media*, C. R. Acad. Sci. Paris, Série I, 333 (2001), pp. 1041–1046.

[11] ——, *Time Reversal and Refocusing in Random Media*, SIAM J. Appl. Math., 63(5) (2003), pp. 1475–1498.

[12] ——, *Stability of time reversed waves in changing media*, to appear in DCDS-B, (2004).

[13] G. Bal and R. Verástegui, *Time Reversal in Changing Environment*, SIAM Mult. Mod. Simul., 2(4) (2004), pp. 639–661.

[14] J. P. Berenger, *A perfectly matched layer for the absorption of electromagnetic waves*, J. Comput. Phys., 114(2) (1994), pp. 185–200.

[15] ——, *Three-dimensional perfectly matched layer for the absorption of electromagnetic waves*, J. Comput. Phys., 127(2) (1996), pp. 363–379.

[16] P. Blomgren, G. Papanicolaou, and H. Zhao, *Super-Resolution in Time-Reversal Acoustics*, J. Acoust. Soc. Am., 111(1) (2002), pp. 230–248.

[17] B. Borcea, G. Papanicolaou, and C. Tsogka, *Theory and applications of time reversal and interferometric imaging*, Inverse Problems, 19 (2003), pp. S139–S164.

[18] B. Borcea, G. Papanicolaou, C. Tsogka, and J. Berryman, *Imaging and time reversal in random media*, Inverse Problems, 18 (2002), pp. 1247–1279.

[19] D. J. Cedio-Fengya, S. Moskow, and M. S. Vogelius, *Identification of conductivity imperfections of small diameter by boundary measurements. Continuous dependence and computational reconstruction*, Inverse Problems, 14 (1998), pp. 553–594.

[20] J. F. Clouet and J.-P. Fouque, *A time-reversal method for an acoustical pulse propagating in randomly layered media*, Wave Motion, 25 (1997), pp. 361–368.

[21] G. C. Cohen, *Higher-Order numerical methods for transient wave equations*, Scientific Computation, Springer Verlag, Berlin, 2002.

[22] R. Dautray and J.-L. Lions, *Mathematical Analysis and Numerical Methods for Science and Technology. Vol.6*, Springer Verlag, Berlin, 1993.

[23] A. C. Davison, *Statistical Models*, Cambridge University Press, 2003.

[24] A. Derode, A. Tourin, J. de Rosny, M. Tanter, S. Yon, and M. Fink, *Taking advantage of multiple scattering to communicate with time reversal antennas*, Phys. Rev. Lett., 90 (2003), p. 014301.

[25] A. Dubois, K. Belkebir, and M. Saillard, *Localization and characterization of two-dimensional targets buried in a cluttered environment*, Inverse Problems, 20 (2004), pp. S63–S79.

[26] G. F. Edelmann, T. Akal, W. S. Hodgkiss, S. Kim, W. A. Kuperman, and H. C. Song, *An Initial Demonstration of Underwater Acoustic Communication Using Time Reversal*, IEEE J. Oceanic Eng., 27 (2002), pp. 602–609.

[27] S. M. Emami, J. Hansen, A. D. Kim, G. Papanicolaou, A. J. Paulraj, D. Cheung, and C. Prettie, *Predicted time reversal performance in wireless communications using channel measurements*, IEEE Comm. Let., (2004).

[28] H. W. Engl, M. Hanke, and A. Neubauer, *Regularization of Inverse Problems*, Kluwer Academic Publishers, Dordrecht, 1996.

[29] M. Fink, *Chaos and time-reversed acoustics*, Physica Scripta, 90 (2001), pp. 268–277.

[30] G. J. Foschini and M. Gans, *On limits of wireless communication in a fading environment when using multiple antennas*, Wireless Personal Communication, 6(3) (1998), p. 311.

[31] J.-P. Fouque and K. Sølna, *Time-reversal aperture enhancement*, SIAM Mult. Mod. Simul., 1 (2003), pp. 239–259.

[32] M. Haider, K. Mehta, and J.-P. Fouque, *Time-reversal simulations for detection in randomly layered media*, Waves Random Media, (2004), pp. 185–198.

[33] W. Hodgkiss, H. Song, W. Kuperman, T. Akal, C. Ferla, and D. Jackson, *A long-range and variable focus phase-conjugation experiment in shallow water*, J. Acoust. Soc. Am., 105 (1999), pp. 1597–1604.

[34] V. Isakov, *Inverse Problems for Partial Differential Equations*, Springer Verlag, New York, 1998.

[35] J. B. Keller, *Stochastic equations and wave propagation in random media*, in Proc. Sympos. Appl. Math., Vol. XVI, Amer. Math. Soc., Providence, R.I, 1964, pp. 145–170.

[36] M. V. Klibanov and A. Timonov, *Carleman Estimates for Coefficient Inverse Problems and Numerical Applications*, Inverse and Ill-Posed Problems Series, VSP, The Netherlands, 2004.

[37] D. Lui, G. Kang, L. Li, Y. Chen, S. Vasudevan, W. Joines, Q. Liu, J. Krolik, and L. Carin, *Electromagnetic Time-Reversal Imaging of a Targer in a Cluttered Environment*, submitted IEEE, (2004).

[38] A. L. Moustakas, H. U. Baranger, L. Balents, A. M. Sengupta, and S. H. Simon, *Communication through a diffusive medium: Coherence and capacity*, Science, 287 (2000), pp. 287–290.

[39] G. Papanicolaou, L. Ryzhik, and K. Sølna, *Statistical stability in time reversal*, SIAM J. App. Math., 64(4) (2004), pp. 1133–1155.

[40] L. Ryzhik, G. Papanicolaou, and J. B. Keller, *Transport equations for elastic and other waves in random media*, Wave Motion, 24 (1996), pp. 327–370.

[41] P. Sheng, *Introduction to Wave Scattering, Localization and Mesoscopic Phenomena*, Academic Press, New York, 1995.